JCI insight

MiRNA-148a-containing GMSC-derived EVs modulate Treg/Th17 balance via IKKB/NF-κB pathway and treat a rheumatoid arthritis model

Jingrong Chen, … , Qing-Ling Fu, Song Guo Zheng

JCI Insight. 2024. https://doi.org/10.1172/jci.insight.177841.

Research In-Press Preview Stem cells

Graphical abstract

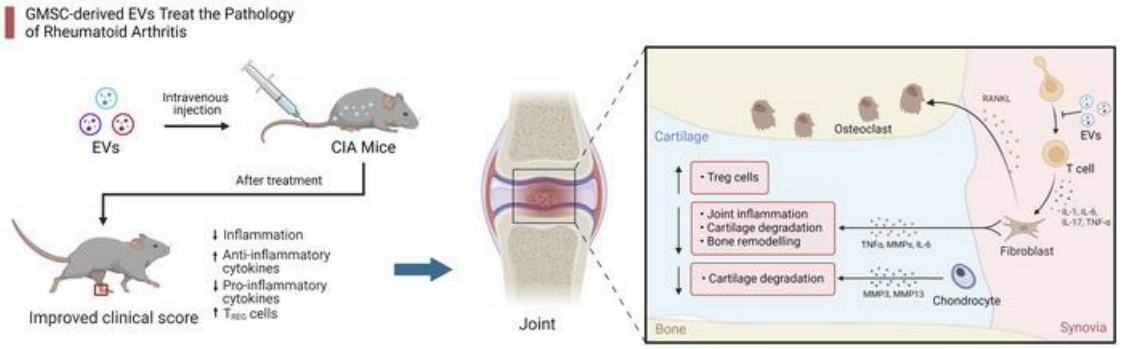

MiRNA-148a-containing GMSC-derived EVs modulate Treg/Th17 balance *via* IKKB/NF-κB pathway and treat a rheumatoid arthritis model

Jingrong Chen[1,2,#], Xiaoyi Shi[2,#], Yanan Deng[1,#], Junlong Dang[1], Yan Liu[2], Jun Zhao[1], Rongzhen Liang[1], Donglan Zeng[3], Wenbin Wu[4], Yiding Xiong[1], Jia Yuan[5], Ye Chen[1,2], Julie Wang[1], Weidong Lin[1], Xiangfang Chen[6], Weishan Huang[7], Nancy Olsen[8], Yunfeng Pan[2], Qingling Fu[9,*] and Song Guo Zheng[1,*]

Running title: GMSC-EVs treat arthritis

[1]Department of Immunology, School of Cell and Gene Therapy, Songjiang Research Institute, Shanghai Songjiang District Central Hospital, Shanghai Jiaotong University School of Medicine, Shanghai, China

[2]Department of Transplantation, Nanfang Hospital, Southern Medical University, Guangzhou, China; Department of Internal Medicine, Division of Rheumatology, The Third Affiliated Hospital of Sun Yat-sen University, Guangzhou, China

[3]Depertment of Clinical Immunology, The Third Affiliated Hospital of Sun Yat-sen University, Guangzhou, China

[4]Department of Spine Surgery, The Third Affiliated Hospital of Sun Yat-sen University, Guangzhou, China

[5]Department of stomatology, The Third Affiliated Hospital of Sun Yat-sen University, Guangzhou, China

[6]Department of Endocrinology, Second Affiliated Hospital of Naval Medical University, Shanghai, China

[7]Department of Pathobiological Sciences, School of Veterinary Medicine, Louisiana State University, Baton Rouge LA, USA

[8]Division of Rheumatology, Department of Medicine, The Penn State University Hershey Medical Center; Hershey PA, USA

[9]Otorhinolaryngology Hospital, The First Affiliated Hospital, Sun Yat-sen University, Guangzhou, China

**Correspondence: Prof. Song Guo Zheng. 768 Zhongshan Middle Road, Shanghai, 201600, China. Tel: +86 21 6772 2300. Email: Song.Zheng@shsmu.edu.cn; Prof. Qingling Fu. 58 Zhongshan second Road, Guangzhou, Guangdong Province, 510030, China. Tel: +86 20 8733 3108. Email: fuqingl@mail.sysu.edu.cn.*

[#]These authors contributed equally to this work.

ABSTRACT

Mesenchymal stem cells (MSCs) have demonstrated potent immunomodulatory properties that have shown promise in the treatment of autoimmune diseases, including rheumatoid arthritis (RA). However, the inherent heterogeneity of MSCs triggered conflicting therapeutic outcomes, raising safety concerns and limiting their clinical application. This study aimed to investigate the potential of extracellular vesicles derived from human gingival mesenchymal stem cells (GMSC-EVs) as a therapeutic strategy for RA. Through *in vivo* experiments using an experimental RA model, our results demonstrated that GMSC-EVs selectively homed to inflamed joints and recovered Treg and Th17 cells balance, resulting in the reduction of arthritis progression. Our investigations also uncovered miR-148a-3p as a critical contributor to the Treg/Th17 balance modulation *via* IKKB/NF-κB signaling orchestrated by GMSC-EVs, which was subsequently validated in a model of human xenograft *versus* host disease (xGvHD). Furthermore, we successfully developed a humanized animal model by utilizing synovial fibroblasts obtained from patients with RA (RASFs). We found that GMSC-EVs impeded the invasiveness of RASFs and minimized cartilage destruction, indicating their potential therapeutic efficacy in the context of RA patients. Overall, the unique characteristics, including reduced immunogenicity, simplified administration, and inherent ability to target inflamed tissues, position GMSC-EVs as a viable alternative for RA and other autoimmune diseases.

KEY WORDS: Mesenchymal stem cells; Extracellular vesicles; Rheumatoid arthritis; Humanized synovial inflammation; IKKB

INTRODUCTION

Rheumatoid arthritis (RA) is a common autoimmune disease characterized by persistent joint inflammation and destruction of cartilage and bone (1, 2). An increasing amount of evidence indicates that mesenchymal stem cells (MSCs) have the potential to fight against autoimmune and inflammatory diseases, including autoimmune arthritis (3-10). However, several concerns arise in clinical practice. For example, MSC in patients are usually dysfunctional, making allogenic MSC transfer the only option, which may trigger immune rejection. Moreover, the long-term cell fate of the transferred MSC in patients remains largely unclear, not to mention common side effects including cellular toxicity and tumorigenesis (11-13). An effective immune therapy depends on precise targeting and potent immune modulation. Current RA treatment regimens involving immune suppressants often require high doses of drugs to show a therapeutic effect in the affected joints, doses which often trigger adverse off-target effects on normal tissues. The current cell-based therapeutic strategies against inflammation often lack homing specificity to the inflamed sites, which limits their applications in the clinic. Developing innovative therapeutic approaches that are devoid of cells and specifically target RA is of utmost importance.

Recent studies identified that many cells exert their function through extracellular vesicles (EVs). There are two main categories of EVs, namely ectosomes and exosomes (14, 15). Ectosomes, which consist of microvesicles, microparticles, and large vesicles ranging from approximately 50 nm to 1 μm in diameter, are formed by outward budding and separate from the plasma membrane. Exosomes, which have a size ranging from 30 to 160 nm, are discharged into the extracellular matrix when the fusion of multivesicular bodies with the plasma membrane occurs (14, 16, 17). Since there is no agreement yet on distinct indicators of EV subcategories, it becomes challenging to differentiate between exosomes or microvesicles. Hence, exosomes or microvesicles are commonly denoted as small EVs, in accordance with the classical references (18-20). According to reports, EVs may facilitate the paracrine impacts of MSCs, enhance tissue healing and immune suppression, and uphold homeostasis (25).

In our current study, we reveal new discoveries that demonstrate the effectiveness of EVs derived from human GMSCs (GMSC-EVs) in treating an animal model of RA. Significantly, microRNA-148a has been recognized as a noteworthy participant in GMSC-EVs, exerting a crucial influence on the suppression of immune response and the reduction of disease progression by specifically modulating the IKKB-NF-κB signaling pathway. Our research

highlights the vast possibilities of GMSC-EVs as an innovative and hopeful treatment without cells to fight against not just RA but also various other autoimmune disorders.

RESULT

Human GMSC-derived EVs suppress T cell activation, proliferation, differentiation and inflammatory cytokines production *in vitro*

GMSCs were analyzed using flow cytometry to investigate the cell surface markers. The findings of our study revealed that GMSCs exhibit the typical traits of MSCs (Supplemental Figure 1A). Differential ultracentrifugation, which is widely adopted for EVs isolation from biological fluids and is therefore considered the "gold standard protocol" of EVs isolation (30, 31). Consequently, the EVs derived from human GMSCs (GMSC-EVs, i. e., G-EVs) were successfully obtained and utilized for subsequent experiments (Figure 1A, Figure 1B, Supplemental Figure 1B, Figure 1C and Supplemental Figure 1B).

To ensure that T cells cultured with GMSC-EVs were not affected by cell apoptosis or death-induced nonspecific reactions, Annexin-V and PI staining was performed. The results demonstrated no overt side effects triggered by GMSC-EVs (Supplementary Figure 2A, B). Furthermore, we examined the interactions between GMSC-EVs and T lymphocytes in a controlled environment and their capability to modulate the proliferation, differentiation, and activity of T cells. The results showed that GMSC-EVs (Green) localized in the cytoplasmic compartment of T cells, indicating their uptake by T cells (Figure 1D). To learn whether GMSC-EVs suppress T cell activation, we examined the expression of the early activation marker CD69 on the T cells. The results demonstrated that GMSC-EVs significantly reduced the proportion of CD69 positive cells in both CD4+ and CD8+ T cell populations, suggesting GMSC-EVs start modulating T cell immune responses since T cells are initially primed (Supplemental Figure 3A, B). In addition, the findings indicated that GMSC-EVs displayed strong inhibitory impacts on the proliferation of CD8+ and CD4+ T cells, as demonstrated by decreased divisions observed through CFSE dilution (Figure 1E). Furthermore, the study found that GMSC-EVs, rather than Fib-EVs, had a significant inhibitory effect on the differentiation of Th17 (CD4+IL-17A+) cells (Figure 1F).

MSC-EVs have been demonstrated to impact the development of Treg cells in a manner that depends on the donor, as indicated by previous studies (32, 33). The research findings indicated that the administration of GMSC-EVs improved the development of FoxP3+ Treg cells when naïve CD4 cells were stimulated under conditions that promote Treg cell polarization (as shown in Figure 1G, H). Additionally, the quantities of inflammatory and non-inflammatory cytokines can function as markers of immune balance. We observed that

co-culturing CD3+ T cells with GMSC-EVs significantly reduced the amounts of TNF-α by CD4+ T cells (Figure 1I). To summarize, our findings indicate that GMSC-EVs hindered the activation, growth, and differentiation of T cells, and suppressed the production of pro-inflammatory cytokines while facilitating the development of regulatory T cells.

Human GMSC-derived EVs improve the collagen-induced arthritis (CIA) model

In our prior investigation, we documented that GMSC greatly improved the pathology and inflammatory reactions in a mouse model of CIA (26). The pathological characteristics of human RA, such as synovial hyperplasia, joint swelling, and damage to bone and cartilage, are largely replicated in this experimental model (34, 35). To extend the prevention potential of GMSC-EVs on inflammatory arthritis, GMSC-EVs were administered to mice at different time points post-immunization (Figure 2A). On day 60 post-immunization, the gross appearance of hind limbs had a significant remission of arthritis in GMSC-EVs treatment mice *versus* that in disease model or Fib-EVs treatment mice (Figure 2B). The consistent foot swelling was noticed and monitored from day 15 to day 60 as indicated in Figure 2C. Moreover, the administration of GMSC-EVs resulted in a postponement of the initiation of arthritic ailment, a decrease in the occurrence of arthritis (Figure 2D), and a reduction in arthritis clinical scores (Figure 2E). Histological analysis revealed that GMSC-EVs treatment resulted in decreased synovial hyperplasia, cartilage damage, and osteoclast activity (Figure 2F, G). In order to assess the level of bone damage in CIA mice, we performed micro-CT scanning and observed a notable safeguarding impact on bone erosion in mice administered with GMSC-EVs (Figure 2H). These results indicate that GMSC-EVs have sufficient therapeutic potency on CIA mice.

Various pieces of evidence indicate that maintaining a proper equilibrium between Th17 cells, which produce IL-17A and promote inflammation, and Treg cells, which are FoxP3+ and inhibit inflammation, is vital in autoimmune arthritis (36, 37). Our research revealed that treatment with GMSC-EVs led to a notable decrease in the occurrence of Th17 cells and a notable increase in the occurrence of Treg cells in the draining lymph nodes (dLNs) (Figure 2I). Additionally, the expression and activity of RORγt, a transcription factor involved in Th17 cell development, were consistently inhibited in GMSC-EVs treated mice (Figure 2J, K). The administration of GMSC-EVs significantly reduced the synthesis of TNF-α by CD4+ cells (Figure 2L), while simultaneously enhancing the release of IL-10, a cytokine known for its anti-inflammatory properties (Figure 2M, N). In addition, GMSC-EVs treatment effectively reduced the levels of pro-inflammatory cytokines TNF-α, IFN-γ, IL-17A, and IL-6 in the blood, while simultaneously increasing the level of the anti-inflammatory cytokine IL-10 (Figure 2O). We found that the introduction of GMSC-EVs also led to a

decrease in the concentrations of autoantibodies in the blood samples (Figure 2P). Collectively, these findings indicate that GMSC-EVs have the ability to improve the pathology and reduce inflammatory responses in a model of inflammatory arthritis.

The distribution of human GMSC-derived EVs in CIA model

In order to precisely determine the anatomical location of transferred GMSC-EVs in the CIA model, we conducted live imaging to analyze the dynamic distribution of GMSC-EVs throughout the entire animal body (Figure 3A). In this study, GMSC-EVs and Fib-EVs were labeled with a lipophilic tracer DiR prior to intravenous injection into CIA mice, and whole body images were obtained 24 hours later. Results indicated that GMSC-EVs homed preferentially to the inflamed joints, whereas Fib-EVs did not (Figure 3B, C). However, concerns have been raised about the accuracy of using lipophilic dye staining for EVs labeling due to potential nonspecific staining of other lipid-containing entities in the extracellular space, formation of dye aggregates or clumps, different metabolism profiles from EVs, etc. To address these issues, mCherry was fused to the COOH-termini of GFP for EVs membrane labeling in our current study, using a CD63-mCherry-GFP lentivirus as an alternative labeling strategy. Consistent with DiR-labeled EV live imaging in CIA mice, we observed that mCherry-carrying GMSC-EVs exhibited a preference for homing to inflamed joints, while Fib-EVs did not (Figure 3D). Notably, GMSC-EVs were found to be stable and able to continuously circulate in inflamed joints after infusion. To monitor this, we conducted a time course analysis at 24 hours, 15 days, and 28 days after injecting DiR-labeled GMSC-EVs into CIA mice. The results showed that a fluorescent signal was still detectable in the joints 28 days after GMSC-EVs injection (Figure 3E). To summarize, our research indicates that GMSC-EVs have remarkable capabilities to migrate towards inflamed joints. Therefore, they might possess considerable promise as a therapeutic alternative for mitigating inflammatory conditions.

Human GMSC-derived EVs exhibited a significant enrichment of miR-148a-3p

EVs have become significant facilitators of cell-to-cell communication, transporting diverse cargo substances like proteins, lipids, mRNAs, and miRNAs to recipient cells, consequently influencing their functions (39). The objective of this research was to determine the precise elements of GMSC-EVs that are accountable for their immunoregulatory capabilities. To achieve this, we performed treatments to eliminate the proteins or RNAs present in GMSC-EVs (Figure 4A). Using these validated RNA-free and/or protein-free GMSC-EVs samples, we observed that the ability of GMSC-EVs to inhibit the production of the proinflammatory cytokine TNF-α depended on the presence of RNAs within GMSC-EVs

(Figure 4B-E). The findings strongly indicate that the RNA transported by GMSC-EVs has a vital function in controlling inflammatory reactions.

To further investigate the molecular composition of GMSC-EVs, we conducted small RNA sequencing to determine their miRNA profiles (Figure 4F). Comparison with Fib-EVs revealed differential expression of 41 upregulated and 10 significantly downregulated miRNAs in GMSC-EVs (Figure 4G). Pathway enrichment analysis using DIANA-MirPath v.3 predicted the potential pathways targeted by these differentially expressed miRNAs, so as to determine the candidate pathways that can be targeted by these miRNAs (Figure 4H). In order to determine the miRNAs that regulate the IKKB/NF-κB signaling pathway, we utilized online prediction resources to generate a list of common miRNAs found in TargetScan, miRWalk, and miRDB. This was illustrated in a Venn diagram, and one of the miRNAs identified was miR-148a-3p (Figure 4I). Following this, our attention shifted to miR-148a-3p. Our biological verification aligned with the bioinformatic discoveries, demonstrating a notable abundance of miR-148a-3p in GMSC-EVs compared to Fib-EVs (Figure 4G, J). In addition, we examined the publicly accessible dataset GSE56649, which consisted of 13 cases of RA and 9 controls without any health issues, in order to discover potential genes associated with the pathophysiology of RA. Our findings indicated a notable increase in the expression of IKKB in RA compared to the controls (as shown in Figure 4K). To sum up, our results indicate that GMSC-EVs regulate the IKKB/NF-κB signaling pathway by means of miR-148a-3p, thus improving the pathology and inflammatory responses linked to inflammatory disorders.

The immunomodulatory functions of human GMSC-derived EVs are attributed to miR-148a-3p

Our investigation focused on determining if GMSC-EVs modulate T cell responses *via* miR-148a-3p. Consistent with expectations, the inhibitory impact of miR-148a-silenced G-EVs (si-G-EVs, Supplemental Figure 4A-C) on the proliferation of CD8+ T cells was less significant when compared to NC-G-EVs, which carry the normal miR-148a-3p (Figure 5A). However, si-G-EVs exhibited limited suppression of Th17 cell differentiation (Figure 5B) and osteoclast formation (Figure 5D, E). In contrast, the activity of miR-148a-3p played a vital role in the promotion of Treg cell differentiation by GMSC-EVs (Figure 5C), suppression of TNF-α production (Figure 5F), and augmentation of IL-10 levels (Figure 5G). In addition, qRT-PCR was performed to evaluate the mRNA expression levels of various transcription factors and cytokines. The results showed that miR-148a-3p plays a crucial role in the ability of GMSC-EVs to induce a tolerant T cell phenotype and inhibit the production of pro-inflammatory cytokines (Figure 5H).

The *in vitro* results, which emphasize the reliance of GMSC-EVs' immunosuppressive role on miR-148a-3p, required further examination of their effects *in vivo*. In order to clarify the essential role of miR-148a-3p in the *in vivo* immunomodulatory function of GMSC-EVs, we performed experiments using a CIA animal model, as described earlier (see Figure 2). In contrast to the beneficial therapeutic effects observed with NC-G-EVs, si-G-EVs demonstrated limited efficacy in delaying the onset of disease, reducing disease incidence (Supplemental Figure 5A), ameliorating clinical scores of arthritic pathology (Supplemental Figure 5B), and mitigating foot swelling (Supplemental Figure 5C). Moreover, si-G-EVs demonstrated limited efficacy in reducing the severity of synovial hyperplasia, damage to the cartilage (Figure 5I), erosion of the bone (Figure 5J), and in regulating the ratio of Th17/Treg cells (Figure 5K). Furthermore, the administration of si-G-EVs did not effectively inhibit the synthesis of pro-inflammatory cytokines like TNF-α, IFN-γ, IL-17A, and IL-6. Moreover, it did not stimulate the generation of the regulatory cytokine IL-10 (Supplemental Figure 5D). Additionally, there was no impact on the levels of autoantibodies (Supplemental Figure 5E). Our results strongly endorse the requirement for miR-148a-3p in the ability of GMSC-EVs to regulate inflammatory reactions and potentially function as a treatment approach for inflammatory disorders.

T-cell response involves the direct targeting of IKKB by miR-148a-3p in GMSC-EVs

Predictions suggest that miR-148a-3p may target IKKB, an important activator of the NF-κB signaling pathway, as certain miRNAs have the ability to bind to the 3’ UTR of IKKB mRNA and regulate its protein expression level (45). We replicated the typical and altered forms of IKKB's 3' UTR into a vector that includes a firefly luciferase reporter gene (Figure 6A). The findings of our study indicated that miR-148a-3p had a substantial impact on the expression of IKKB, which was influenced by the 3' UTR (as shown in Figure 6B). In order to validate that miR-148a-3p directly targets IKKB at the endogenous expression level, we transfected HEK-293T cells with the miR-148a-3p mimic for 48 hours and examined the mRNA levels of IKKB. In Figure 6C, a notable reduction in IKKB mRNA levels was noted in cells that were subjected to treatment with the miR-148a-3p mimic. In the same way, the levels of p-IKKB and IKKB proteins were significantly reduced in cells that received the miR-148a-3p mimic treatment (Figure 6D). To confirm the essential role of miR-148a-3p in the targeting and modulation of IKKB expression in activated CD3+ T cells by GMSC-EVs, we examined the impact of miR-148a obtained from GMSC-EVs on IKKB in T cells. The findings of our study revealed that NC-G-EVs effectively decreased the expression of IKKB, whereas si-G-EVs did not have an impact on the levels of IKKB and NF-κB at either the mRNA or protein levels (Figure 6E, F).

miR-148a-3p is utilized by EVs derived from human GMSCs to improve xGvHD

To investigate whether the short-term rebalancing of human Treg and Th17 cells by GMSC-EVs and the crucial role of miR-148a-3p derived from GMSC-EVs in suppressing T cell immune responses *in vitro* have similar long-term consequences *in vivo*, we used a xenograft *versus* host disease (xGvHD) model where human T cells are adoptively transferred into the immunodeficient mice and human cells were activated by animal antigens (Figure 7A). Initially, we used the DiR-labeling method mentioned earlier to track the dynamic distribution of GMSC-EVs in the xGvHD mice. After 24 hours of adoptive transfer, we detected DiR-labeled EVs in various organs including the spleen, lymph nodes, intestine, kidneys, liver, and lungs. The spleen, lymph nodes, and intestine showed a higher abundance of GMSC-EVs compared to Fib-EVs, whereas both types of EVs primarily accumulated in the liver and lungs (Figure 7B, C).

Furthermore, we assessed if GMSC-EVs could mitigate xGvHD development and investigated the involvement of miR-148a-3p in this mechanism. We observed that the xGvHD positive control mice exhibited significant mortality (refer to weight loss in Figure 7D and survival data in Figure 7E). Moreover, these mice showed an expansion of T cells (weekly blood phenotype displayed in Figure 7F, and typical percentages of CD3+ T cells in dLNs at day 50 shown in Figure 7G). Nonetheless, the characteristic indications of xGvHD were significantly lessened when NC-G-EVs carrying normal miR-148a-3p were administered, whereas the administration of si-G-EVs lacking miR-148a did not yield similar outcomes. On the 50th day, we gathered different body parts from the xGvHD mice and examined the histopathological ratings of the lungs, liver, and intestines to assess the curative impacts of GMSC-EVs. According to our results, NC-G-EVs effectively decreased the histopathological scores in the various organs of the xGvHD mice. However, si-G-EVs did not successfully reduce lymphocyte infiltration or the associated pathological scores in the lungs, liver, and intestine (Figure 7H). The systemic production of pro-inflammatory cytokines is a notable characteristic of xGvHD. Hence, we assessed the concentrations of different cytokines in the blood samples. As anticipated, NC-G-EVs effectively suppressed the synthesis of inflammatory cytokines including TNF-α, IL-2, IFN-γ, IL-17A, and IL-4, while enhancing the generation of IL-10. Conversely, these cytokine levels returned to untreated disease levels in the si-G-EVs treated group (Figure 7I).

Human GMSC-derived EVs hinder the migration of RASFs and prevent them from damaging cartilage in the humanized animal model of inflammatory synovial fibroblast-mediated arthritis

This research project involved the creation of a humanized animal model that accurately replicates the inflammatory synovial fibroblast-mediated process observed in humans, thus effectively simulating synovial inflammation. In order to clarify if GMSC-EVs can prevent cartilage damage by controlling the aggressiveness of synovial fibroblasts, we conducted a transplantation of synovial fibroblasts from patients with RA (RASFs) into severe combined immunodeficiency (SCID) mice to induce synovitis inflammation similar to that in humans, which is mediated by RASFs (Figure 8A). To track the migration of RASFs, we initially labeled them with a red fluorescent dye called DiI, and subsequently implanted the labeled RASFs along with healthy cartilage and therapeutic GMSCs or GMSC-EVs in contralateral sites of mice at day 15. At day 60, both the primary cartilages without direct exposure to RASFs were removed, and fluorescence microscopy revealed a significant lower fluorescence signal of RASFs in the primary cartilages of GMSC and GMSC-EVs-treated mice, indicative of the ability of both GMSCs and GMSC-EVs to suppress RASFs migration to distant sites *in vivo*. In contrast, the primary cartilages of GMSC-EVs-treated mice exhibited a slightly reduced fluorescence signal in RASFs compared to mice treated with GMSCs (Figure 8B, C). Moreover, the histopathological analysis with H&E staining revealed that RASFs were capable of infiltrating the cartilage and inducing significant erosion in the opposing cartilages (Figure 8D). Notably, it was observed that the main cartilage, even without direct contact with RASFs, exhibited comparable deterioration, suggesting the ability of RASFs to migrate to a remote location in living organisms (Figure 8E). Notably, both GMSCs and GMSC-EVs effectively attenuated lymphocyte infiltration and minimized cartilage destruction in both contralateral and primary cartilages (Figure 8D, E). This observation suggests that GMSC-EVs exert direct beneficial effects not only in the local cartilage but also in cartilage that is not directly affected by RASFs. Collectively, these findings affirm that GMSC-EVs impede the invasiveness of RASFs, ultimately safeguarding against cartilage destruction *in vivo*.

DISCUSSION

MSCs are currently being investigated in many clinical trials either alone or in combination with scaffolds or biomolecules of different types. In recent years, a new group of MSCs named GMSCs has been discovered. Our team, along with other teams, has shown the powerful ability of GMSCs to modulate the immune system in various animal models of human ailments (26, 28, 48-54). Nevertheless, the lack of a uniform MSC phenotype arises from the considerable diversity of MSCs, posing challenges in formulating standardized operational procedures (SOPs) for the clinical utilization of MSCs. EVs prepared from MSCs are highly controllable and can be made consistently without any stimulation over the parent MSCs, allowing the development of an SOP in the clinic. GMSCs have unique advantages

that give them a favorable position. These advantages encompass an easily accessible source devoid of substantial trauma, swifter proliferation kinetics, and an absence of tumorigenicity risks during cell culture, as evidenced by previous investigations (55-57). These inherent benefits position GMSCs as an exemplary candidate for the generation of MSC-EVs on a mass scale.

EVs often function as transporting cargos, essentially as an intercellular shuttle to deliver biological components such as proteins and RNAs from effector cells to their target cells. MSC-EVs can modulate both innate and adaptive immunity (58). Significantly, recent inquiries have emphasized the healing effectiveness of MSC-EVs in addressing autoimmune disorders through proficiently restraining the activation of T effector cells. Consequently, MSC-EVs have garnered attention as a promising cell-free therapeutic approach (59-62). Within the context of an autoimmune disease, we utilized a CIA model to investigate the immune-modulatory capabilities of GMSC-EVs in this study. Our results unequivocally demonstrate that adaptively transferred GMSC-EVs significantly delay the onset of arthritis and improve clinical symptoms. Moreover, the development of Th17 cells, along with the simultaneous decrease in FoxP3+ Treg cells, has been linked to the onset of RA (63, 64). In humans, the ratio of Th17 to Treg has been identified as a distinct biomarker for the progression of RA. Our current research results confirm that the transfer of GMSC-EVs effectively regulates the activation and growth of self-reactive Th17 cells, while simultaneously promoting the expansion of Treg cells in mice with CIA. Our findings also reveal that GMSC-EVs reduce the levels of pro-inflammatory cytokines, while notably enhancing the production of IL-10. These findings align with previous studies on the immunomodulatory effects of MSCs-EVs (67-69). Collectively, our data indicate that the therapeutic efficacy of GMSC-EVs lies in their ability to tip the scales in favor of suppressing inflammatory responses while retaining immunosuppressive activity, thereby reducing the risk of developing arthritis.

Compared with conventional animal models, an anthropogenic animal model can mimic human immune disorders. The humanized animal model is the best *in vivo* model before clinical trials, to determine whether GMSC-EVs have the immunomodulatory efficacy of inflammation *in vivo* before a clinical trial. Xenogeneic Human (graft) *versus* mouse (host) disease (xGvHD) is established through intravenous injection of healthy peripheral blood lymphocytes into NOD/SCID mice. The development and severity of GvHD disease were determined by analyzing the survival, weight changes, organ infiltration of inflammatory cells, pathology, serum IgG and cytology. In our recent investigation, we discovered that GMSC-EVs specifically targeted the inflamed organs and reduced the survival and

progression of xGvHD, suggesting the potential translational significance of GMSC-EVs in treating inflammatory diseases mediated by human immune cells. These results underscore the potential clinical translational value of GMSC-EVs.

However, before conducting clinical trials with GMSC-EVs on patients with RA, it is crucial to utilize a humanized animal model that involves inflammation synovial cells and accurately reproduces the bone and cartilage damage features observed in RA. By utilizing this, researchers will be able to definitively establish the effectiveness of GMSC-EVs within the framework of patients with RA. The established model for studying migration and invasion of RASFs in SCID mice has previously proven to be a useful tool for preclinical research, offering significant insights and opportunities for advancements in the clinical feasibility (70, 71). In this model, RASFs could travel in SCID mice from an inflamed cartilage implant to an un-inflamed site (70, 72). We have previously utilized this humanized model to explore the regulatory role of T cells in inflammatory synovitis (37, 73). During our current investigation, we made a fascinating finding that GMSC-EVs hindered the ability of RASFs to invade, ultimately offering a defense against cartilage degradation, whether or not it is seeded with RASFs. Employing this model, we have conducted a comprehensive evaluation of the protective effects exerted by GMSC-EVs and GMSCs on cartilage damage in the context of synovial inflammation. Furthermore, we have explored the capability of GMSC-EVs and GMSCs to inhibit the physiological function of human inflammatory synovial tissue.

A direct quantitative relationship between GMSCs and GMSC-EVs remains elusive, but approximately 5 million GMSCs are required to generate 100 μg of GMSC-EVs. In the inflammation synovial cell-mediated humanized animal model, 2×10^6 GMSCs and 100 μg of GMSC-EVs were used. Although current results revealed that no statistically significant disparity in the impediment of RASFs invasion or the preservation of cartilage damage was observed between 2×10^6 GMSCs and 10 million GMSC-generated EVs. However, it is important to underscore that autologous MSCs, typically functionally impaired in MSC cell therapy applications, often necessitate employment of allogeneic cells. Moreover, the quantity of MSCs that can be infused simultaneously is restricted to a predetermined threshold, thereby mandating multiple infusions to sustain or regenerate functional activity. The requirement for multiple infusions poses challenges to the autologous transplantation of cultured cells, raising the specter of uncertain differentiation and cellular distortion. Additionally, even if autologous MSCs exhibit normal functionality, autologous MSCs transplantation becomes extremely challenging in the event of an acute illness due to the time-consuming process of cell preparation and transplantation. In stark contrast, cell-free

therapy utilizing MSC-derived EVs represents a distinct modality. This approach boasts minuscule immunogenicity and circumvents the obstacles associated with allogeneic transplantation rejection. MSC-EVs can be prepared proactively, endowing them with an advantageous edge in the management of emergent cases. Furthermore, administration of high-dosage EV infusions does not engender adverse effects. Consequently, the unparalleled biological attributes exhibited by GMSC-EVs confer advantages in mitigating autoimmune diseases such as RA, surpassing the capabilities of their GMSC counterparts.

In recent times, an increasing amount of proof indicates that MSC-EVs possess the ability to specifically target various organs or cell types, which is contingent upon the presence of damaged or inflamed tissues. Conversely, MSCs could be mostly trapped in the lungs, given the size of MSCs, the lung barrier of the hosts, and the lifespan of MSCs *in vivo* post administration (74, 75). EVs exhibit a buoyant density ranging from 1.1 to 1.18 g/Ml when subjected to a sucrose density gradient. Lipid rafts in their membranes are enriched with cholesterol, sphingomyelin, ceramide, and other substances (76, 77). During the formation of multivesicular bodies (MVB), the EVs membrane undergoes invagination, resulting in EVs acquiring the identical membrane orientation as the host cell membrane. MSC-derived EVs have the ability to readily cross any physiological barrier due to their nanoscale size, thereby enhancing their uptake efficiency by target tissues (17). A recent study reported a greater uptake specificity of MSCs-EVs for the injured kidney (78). The study successfully showcased the selective migration and circulation of GMSC-EVs to the inflamed joints in a mouse model of RA, as well as to inflamed lesions in a humanized model of xGvHD. Additionally, Shen B et al. provided insights into the role of MSC-derived exosomes expressing high levels of CCR2 in the context of renal ischemia/reperfusion injury in mice. They observed a reduction in CCL2 levels, which in turn diminished the recruitment and activation of macrophages in the injured area (79). Complementing these findings, our unpublished data indicate a higher expression of CCR2, CCR7, CCR5, and CXCR5 in GMSC-EVs. These observations underscore the necessity for a more precise understanding of the mechanisms driving inflammatory homing. The potential application of this phenomenon in treating diseases characterized by physiological barriers, such as RA and multiple sclerosis (MS), warrants further exploration.

EVs act as carriers to package proteins, lipids, mRNAs, and regulatory miRNAs derived from parent cells, and transport them to target cells in order to regulate their functions (39, 80). The identification of miRNA and proteins in GMSC-EVs and their role in modulating target cells, along with the associated mechanisms, remains unexplored. It is also highly possible that either miRNAs or proteins are involved in immune modulation of MSC-EVs. miRNA, a

type of small noncoding RNAs, regulates gene expression after transcription by specifically binding to the 3' UTR region of target gene mRNA. This binding leads to destabilization of the mRNA and decreased protein expression levels of the target genes (81). MSC-EVs contain specific miRNAs that play roles in various physiological and pathological processes, including tissue regeneration, epigenetic alteration, immunomodulation, and tumorigenesis. Significantly, EVs with a membranous composition function as carriers of miRNAs, transporting operational miRNAs into specific cells. According to the report, MSC-EVs were capable of partially preventing allergic airway inflammation by delivering miR-146a-5p (82). MiR-155 and miR-146a are the most extensively researched miRNAs in immune responses associated with RA. They are of particular interest in clinical settings due to their detectability in whole blood, which makes them both relevant and feasible (83). MiR-146 has demonstrated its involvement in the regulation of interleukin-1 receptor-associated kinase 1 and 2 (IRAK1 and IRAK2), both of which play a crucial role in toll-like receptor (TLR) signaling and NF-κB transcriptional activities (84, 85). High levels of the proinflammatory cytokine TNF-α in the peripheral blood are attributed to the excessive expression of miR-146a. The precise molecular mechanisms by which miR-146a operates to regulate the development and advancement of RA remain unknown.

During this research, we have made a significant discovery that miRNAs, instead of proteins, play a vital role as signaling mediators in GMSC-EVs to control the activities of target cells. In particular, we discovered that miR-148a-3p is abundantly present in GMSC-EVs and plays a crucial part in the immunomodulatory characteristics associated with GMSC-EVs. The initiation of the inflammatory cascade is greatly influenced by the activation of the NF-κB signaling pathway. Persistent activation of the NF-κB pathway has been implicated in various inflammatory disorders. This study shows that miR-148a-3p, present in GMSC-EVs, plays a crucial role in regulating T cells by directly inhibiting the activation of the IKKB-NF-κB signaling pathway. Blocking the expression of endogenous miR-148a-3p in GMSC-EVs led to the loss of their capacity to inhibit IKKB and NF-κB activity and regulate the equilibrium between Th17 and Treg cells.

Translational applications can greatly benefit from the numerous advantageous traits exhibited by EVs originating from MSCs. The establishment of a standardized, scalable cell culture method and robust EVs isolation techniques that consistently yield immunomodulatory EVs are pivotal for developing reliable SOPs for MSC-EV-based cell-free immunotherapy in a clinical setting. Additional investigation is necessary to improve our comprehension of the healing capabilities of MSC-EVs and uncover the molecular processes linked to their formation, variety, and specificity. Currently, MSCs are the only

human cell type known to possess the ability for large-scale production of EVs, making them an attractive source for generating GMSC-EVs. GMSC-EVs harbor abundant bioactive materials within their cargo or on their surface, endowing them with significant therapeutic potential and desirable attributes as vehicles for drug delivery. Overall, our study illuminates the substantial potential of GMSC-EVs in the realm of cell-free immunotherapy, positioning them as the prime contender for extensive production of therapeutic EVs targeting RA disease. By harnessing the beneficial characteristics of GMSC-EVs, such as their reduced immunogenicity, simplified administration, and inherent ability to target inflamed tissues, GMSC-EVs emerge as a viable alternative for RA and other autoimmune diseases.

METHODS

Sex as a biological variant. Both male and female mice were utilized in this study as we had previously determined that no significant differences in exist between the two sexes regarding the outcomes reported in our manuscript.

Ethics statements. The study was conducted following the guidelines of the Declaration of Helsinki by the World Medical Association. GMSCs were isolated and cultured from human tissues obtained from healthy donors who underwent wisdom teeth surgery at the Third Hospital at the Sun Yat-sen University in China, and the School of Cell and Gene Therapy at the Shanghai Jiaotong University School of Medicine in China with informed consents.

Mice. DBA/1 J, NOD/SCID, and C57BL/6J mice were acquired from Charles River Laboratories in Beijing, China. The animal research was conducted following the guidelines of the animal use protocol, which received approval from the Institutional Animal Care and Use Committee of each institute as mentioned earlier. The experiments adhered to all guidelines, both institutional and national, for the care and utilization of laboratory animals, with mice aged between 6 and 13 weeks being employed.

*The suppression assay of T-cell proliferation, differentiation and cytokine production in vitro***.** CD3+ T lymphocytes derived from C57BL/6J mice of the wild type were isolated through the employment of the AutoMACS system, manufactured by Miltenyi Biotec. Afterwards, the cells were marked with carboxyfluorescein succinimidyl ester (CFSE, 1μM). Afterwards, the T cells labeled with CFSE were incubated with EVs at a concentration of 20 μg/mL. In the co-culture, antigen-presenting cells (APCs) treated with mitomycin C were also present, with a ratio of 1:1, along with a soluble anti-CD3 antibody at a concentration of 0.05 μg/mL. Following a period of 72 hours, the cells were gathered and subjected to flow cytometry

analysis to examine the CFSE dilution in CD8+ and CD4+ T cells. The anti-CD3 antibody used in this experiment was purchased from BioLegend.

To conduct the T-cell differentiation test, untainted CD4+CD62L+ T cells were extracted from the spleens of C57BL/6J mice of the wild type using the AutoMACS system, ensuring a purity level exceeding 95%. The CD4 cells, which were inexperienced, were cultured using Th17 (soluble anti-CD3, 1 μg/mL; soluble anti-CD28, 1 μg/mL; rmIL-6, 20 ng/mL; rmTGF-β, 2 ng/mL; anti-IFN-γ, 5 μg/mL; anti-IL-12, 5 μg/mL; and anti-IL-4, 5 μg/mL) and Treg (soluble anti-CD3, 1 μg/mL; soluble anti-CD28, 1 μg/mL; rmTGF-β, 2 ng/mL; and rhIL-2, 30-50 U/mL) inductive conditions. This was done in the presence of mitomycin C-treated APCs at a 1:1 ratio for a period of 3 days. Flow cytometry was utilized to determine the proportion of Th17 (CD4+IL-17A+) and Treg (CD4+FoxP3+) cells. BioLegend provided the anti-CD3 and anti-CD28 Abs, and R&D supplied the recombinant cytokines IL-6, IL-2, and TGF-β. Furthermore, BioLegend provided us with antibodies against IFN-γ, IL-12, and IL-4.

In order to examine the production of cytokines, we isolated splenic CD3+ T cells from wild type C57BL/6J mice using the AutoMACS system, ensuring a purity level exceeding 95%. The cells were grown in a 48-well plate with a density of 2 million cells per well. They were then treated with soluble anti-CD3 (1 μg/mL) and soluble anti-CD28 (1 μg/mL) antibodies. Following a 72-hour incubation period, the cells were collected and the secretion levels of TNF-α and IL-10 were examined utilizing flow cytometry.

Establishment of collagen-induced arthritis (CIA) model. Freund's incomplete adjuvant (IFA) mixed 3 mg/mL heat-denatured *Mycobacterium* (Chondrex) with bovine type II collagen (C-II, 4 mg/mL) in an equal volume, resulting in an emulsion of C-II at a concentration of 3 mg/Ml. As previously mentioned (34), DBA-1J mice were immunized by injecting 100 μL/mouse C-II mixture intradermally at the tail's base. The CIA model, which is induced by collagen, is extensively employed for the examination and assessment of the pathological mechanism of potential autoimmune disorders (87). During the experiment, a single mouse was administered EVs in 100 μL of PBS at a concentration of 1 μg/μL through intravenous injection on day 0, 15, and 30. Clinical scores of arthritis features were evaluated every 2-3 days to determine arthritis incidence. Arthritis severity of every mouse was assessed and rated individually, following the previously mentioned protocols (35, 88, 89). The scores for each paw were added together to calculate a total arthritis severity score per mouse, with a maximum score of 16 for each mouse. The evaluation of each paw score was done in the following manner: 0 indicates the absence of arthritis symptoms, 1 indicates slight swelling limited to the tarsal bones or ankle joint, 2 indicates slight swelling extending from the ankle

to the tarsal bones, 3 indicates moderate swelling extending from the ankle to the metatarsal joints, and 4 indicates severe swelling encompassing the ankle, foot, and digits, or limb ankylosis. The thickness of paw swelling was measured every 2-3 days. Mice were euthanized on the 60th day using CO_2 inhalation and cervical dislocation. Histopathological examination was performed on the collected joint specimens, while micro-computed tomography (micro-CT) analysis was conducted on the hind limb paws. The severity of synovitis, pannus development, and bone/cartilage damage was assessed using a graded system, as outlined: grade 0 indicates the absence of inflammation, grade 1 indicates mild inflammation with synovial lining thickening but no cartilage damage, and grades 2-4 represent escalating levels of inflammatory cell infiltration and cartilage/bone destruction. The investigators, who were unaware of the experimental conditions, assessed clinical scores, arthritis occurrence, paw thickness, and histological scores.

Histological evaluation. Mice tissues were gathered and preserved using 10% formalin. They were then sliced into 4-7 μm sections, followed by a 30-minute exposure to a constant temperature oven set at 65 °C. Afterward, the sections were soaked in xylene I for 15 minutes, followed by a 15-minute soak in xylene II. After slicing, the specimens were treated sequentially with 100% ethanol, 95% ethanol, 85% ethanol, and 75% ethanol for a duration of 5 minutes each. Subsequently, they were rinsed with flowing water for a period of 10 minutes. Sections were treated with hematoxylin aqueous solution for a duration of 5 minutes followed by eosin (H&E) staining solution for a period of 1-2 minutes. To evaluate the cartilage matrix, toluidine blue staining was conducted, while tartrate acid resistant phosphatase (TRAP) staining was carried out to measure the distribution of osteoclasts. Microscopic sections were photographed to obtain histologic images. A semiquantitative scoring system, as previously explained (90), was used to assess the histological characteristics of CIA, which encompassed synovial hyperplasia, infiltration of inflammatory cells, destruction of cartilage, and erosion of bone. Investigators who were unaware of the experimental conditions evaluated all slides.

Micro-CT analysis of bone erosion. Hind paws were removed for CT analysis as described previously (27). In short, the scans were conducted using a 3.6 mm length that covered the entire individual paw. The scans were performed with the given parameters: a voxel size of 17.5 μm, 55 kV, 145 μA, an integration time of 200 ms, and 211 image slices. The pictures were transformed into 8-bit and imported into Mimics software (Materialise, Belgium). They were then filtered using discrete Gaussian filtering with a variance of 1 and a maximum kernel width of 1. Consequently, the micro-CT system (Viva CT 40, Scanco, Switzerland) was used to obtain high-resolution three-dimensional images of hind paws' bones. Bone

erosion was quantified by using volumes of interest located at the paw. Consistently, the areas of focus were aligned with the 3D longitudinal axis of the third metatarsal, and the volumes of the second through fourth metatarsal and phalangeal bones were computed.

In vivo Optical imaging (OI). Mice were intravenously administered with DiR-labelled or mCherry-carried EVs, equivalent to a dose of 100 μg. EVs were injected at various time intervals to examine their biodistribution in live organisms. Using the Bruker in Vivo MS FX PRO Imager (Bruker, Billerica, MA, USA) and the IVIS 200 small animal imaging system (PerkinElmer, Waltham, MA, USA), the mice were imaged. The Ex filter at 700 nm and the Em filter at 780 nm (DIR) were used, along with the Em filter at 530 nm and the Em filter at 620 nm (mCherry). To establish a background measurement, the fluorescence originating from the background was measured and subsequently subtracted. The Em fluorescence was standardized to photons per second per square centimeter per steradian (p/sec/cm2/sr). The color picture displays the arrangement of fluorescence across the creature superimposed on monochrome pictures of the mice, which were gathered simultaneously. The acquisition and analysis of images were performed using Living Image 4. 0 software (PerkinElmer), as previously explained (91). The average radiance ± SD was used to express the data. Following the completion of the experiments, the mice were euthanized and the tissues (including lymph nodes, spleen, kidney, liver, lung, and intestine) were promptly imaged using the aforementioned method.

Dual luciferase reporter gene assay. The miR-148a-3p and IKKB putative binding sites were predicted using the biological website (*http //www. targetscan. org*), and their interaction was confirmed through a dual luciferase reporter gene assay. The renilla luciferase and firefly luciferase dual luciferase reporter gene in the pEZX-MT05 vector (GenePharma, Shanghai, China) had a cloned fragment of the IKKB wild-type (WT) and mutant (MT) 3' UTR downstream. Next, WT or MT IKKB 3' UTR reporter plasmids were co-transfected into HEK 293T cells with the miR-148a-3p mimic or miRNA negative control (mi-NC) using Lipofectamine 3000 (Thermo, MA, USA) as instructed by the manufacturer. The Dual-Luciferase® Reporter Assay System (Promega, Madison, WI) was utilized to measure luciferase activity, following the guidelines provided by the manufacturer. The luciferase activities were standardized based on the renilla luciferase activity.

Xenogeneic graft versus host disease (xGvHD). After receiving 2.5 cGy total body irradiation from Rs2000 (Rad Source, USA) (47, 92). NOD-SCID mice were intravenously administered with 20×10^6 human PBMCs depleted of CD25. EVs were transfused intravenously in a volume of 100 μL PBS at a concentration of 1 μg/μL after a delay of 2-4 hours, on day 0, 15,

and 30, respectively. Survival was checked daily. Weight and GvHD score were monitored every 2-3 days. Blood sample was collected once a week to test the expression of human CD3+ cells. Mice were euthanized on the 50th day using CO_2 and cervical dislocation. Liver, lung and intestine isolated from mice were applied for H&E staining as described above. The assessment of the inflammation level in the liver, lung, and intestine was determined using the following criteria: 0 indicates the absence of any inflamed digits, 1 indicates 1 to 5 inflamed digits, 2 indicates 6 to 10 inflamed digits, 3 indicates 11 to 15 inflamed digits, and 4 indicates 16 or more inflamed digits. The investigators who were unaware of the experimental conditions assessed the histological scores. ELISA analysis was performed on serum samples to detect the cytokines TNF-α, IFN-γ, IL-2, IL-4, IL-17, and IL-10. Flow cytometry analysis was performed using peripheral blood to determine the percentage of CD3+ cells in humans. Liver, lung and intestine were applied for pathological examination.

Inflamed synovial fibroblast-mediated humanized animal model. On the 0th day, a surgical procedure was performed on severe combined immunodeficiency (SCID) mice involving dorsal skin. Anesthesia was induced using isoflurane, followed by a sterile incision made with surgical scissors. To minimize discomfort, bupivacaine was topically applied. Subsequently, a spongiform complex consisting of healthy donor cartilage tissue was implanted as the primary graft. Patients at The Third Affiliated Hospital of the Sun Yat-sen University and The Shanghai Jiaotong University School of Medicine were required to provide written informed consent before reaching this stage. Synovial fibroblasts (RASFs) obtained from patients with RA were cultured and stained with the CM-DiI red fluorescent labeling kit (ThermoFisher Scientific) according to the instructions provided by the manufacturer. To label the cells, they were incubated in the CM-DiI/PBS solution at a temperature of 37 °C in a dark environment for a duration of 5 minutes, and then kept at 4 °C for 15 minutes. Afterwards, the cells that had been labeled were rinsed with 1× PBS and then suspended in a new medium. On the 15th day, the final RASFs and a segment of healthy donor cartilage tissue encapsulated within a spongiform complex were implanted into the contralateral dorsal skin of SCID mice, serving as the contralateral implant. Either 2×10^6 GMSCs in 100 μL of PBS or 100 μg of GMSC-EVs in 100 μL of PBS were injected into the contralateral spongiform complex. On the 60th day, euthanasia was performed using CO_2 followed by cervical dislocation. The main and opposite implants (containing cartilage tissue) were extracted, and a section of the cartilage was placed in optical coherence tomography (OCT) compound and frozen at -80 °C. Using a Lab-Tek tissue processor (Leica, Solms, Germany), sections with a thickness of around 50 nm were acquired from the cartilage tissues. The fluorescence microscope was utilized to assess the fluorescence intensity of CM-DiI-labeled RASFs. Additionally, the excised cartilage from both contralateral and

ipsilateral implants was subjected to standard H&E staining. Invasion scores and cartilage degradation were determined according to a previously reported classification system (93).

Statistical analysis. The data were presented in the form of mean ± SD. Means between two groups were compared using a two-tailed Student's t-test. One- or two-way analysis of variance (ANOVA) was utilized to examine variations in the averages across several groups. Kaplan-Meier curves were used to plot survival curves and then analyzed using log-rank tests. Statistical significance was determined by analyzing the data with GraphPad Prism Software (version 9. 3), considering p values less than 0.05, 0.01, 0.001, and 0.0001.

Study approval. All patients' informed consent were obtained. The study protocol and the use of the material was approved by the Third Hospital of Sun Yat-sen University in China, and the School of Cell and Gene Therapy at the Shanghai Jiaotong University School of Medicine in China.

Data availability. All data are included in the Supporting Data Values file. Any data that support the findings of this study are available from the corresponding authors upon reasonable request. The RNA-seq data, quality control information and cluster information are available at the NCBI's Gene Expression Omnibus (GEO) data repository with the accession number GSE262961 (https://www.ncbi.nlm.nih.gov/geo/query/acc.cgi?acc=GSE262961).

AUTHOR CONTRIBUTIONS

JRC and XYS performed experiment and analyzed data; JRC, XYS and WSH wrote the manuscript; XYS, YND, JLD, YL, JZ, RZL, DLZ, WBW, YDX, YC, JW, WDL, and XFC helped in data collection; DLZ and JY helped in the collection of gingival tissues; XYS and YND helped in data analysis and revised manuscript; NO, WSH, YFP and QLF helped in manuscript editing; SGZ conceptualized the research, designed experiments, analyzed data and finalized the manuscript for submission.

FUNDING

This study was supported by the National Key R&D Program of China (2017YFA0105801), the Youth Program of National Natural Science Foundation of China (82201999, 82304975 and 82001760), the General Program of China Postdoctoral Science Foundation (2021M693608), the Guangdong Basic and Applied Basic Research Foundation (2023A1515010002) and the Guangzhou Basic and Applied Basic Research Foundation (202201011085).

DECLARATION OF INTERESTS

The authors declare no competing interests.

ACKNOWLEDGEMENTS

We sincerely thank Guangzhou Blood Center (31 Luyuan Road, Guangzhou, China) for kindly providing us with buffy coats of human volunteers.

REFERENCES

1. Zou Y, et al. Long noncoding RNA LERFS negatively regulates rheumatoid synovial aggression and proliferation. *J Clin Invest*. 2018;128(10):4510-4524.
2. Liu Y, et al. uPAR promotes tumor-like biologic behaviors of fibroblast-like synoviocytes through PI3K/Akt signaling pathway in patients with rheumatoid arthritis. *Cell Mol Immunol*. 2018;15(2):171-181.
3. Uccelli A, Moretta LPistoia V. Mesenchymal stem cells in health and disease. *Nat Rev Immunol*. 2008;8(9):726-36.
4. Zappia E, et al. Mesenchymal stem cells ameliorate experimental autoimmune encephalomyelitis inducing T-cell anergy. *Blood*. 2005;106(5):1755-61.
5. Ponte AL, et al. The in vitro migration capacity of human bone marrow mesenchymal stem cells: comparison of chemokine and growth factor chemotactic activities. *Stem Cells*. 2007;25(7):1737-45.
6. Gonzalez-Rey E, et al. Human adult stem cells derived from adipose tissue protect against experimental colitis and sepsis. *Gut*. 2009;58(7):929-39.
7. Sui W, et al. Hematopoietic and mesenchymal stem cell transplantation for severe and refractory systemic lupus erythematosus. *Clin Immunol*. 2013;148(2):186-97.
8. Karussis D, et al. Safety and immunological effects of mesenchymal stem cell transplantation in patients with multiple sclerosis and amyotrophic lateral sclerosis. *Arch Neurol*. 2010;67(10):1187-94.
9. Augello A, et al. Cell therapy using allogeneic bone marrow mesenchymal stem cells prevents tissue damage in collagen-induced arthritis. *Arthritis Rheum*. 2007;56(4):1175-86.
10. Aggarwal SPittenger MF. Human mesenchymal stem cells modulate allogeneic immune cell responses. *Blood*. 2005;105(4):1815-22.
11. Chamberlain G, et al. Concise review: mesenchymal stem cells: their phenotype, differentiation capacity, immunological features, and potential for homing. *Stem Cells*. 2007;25(11):2739-49.
12. Breitbach M, et al. Potential risks of bone marrow cell transplantation into infarcted hearts. *Blood*. 2007;110(4):1362-9.
13. Bifari F, et al. Immune Modulation by Mesenchymal Stem Cells. *Transfus Med Hemother*. 2008;35(3):194-204.
14. Colombo M, Raposo GThery C. Biogenesis, secretion, and intercellular interactions of exosomes and other extracellular vesicles. *Annu Rev Cell Dev Biol*. 2014;30(255-89.
15. Kalluri RLeBleu VS. The biology, function, and biomedical applications of exosomes. *Science*. 2020;367(6478):
16. Mathivanan S, Ji HSimpson RJ. Exosomes: extracellular organelles important in intercellular communication. *J Proteomics*. 2010;73(10):1907-20.
17. Kowal J, Tkach MThery C. Biogenesis and secretion of exosomes. *Curr Opin Cell Biol*. 2014;29(116-25.
18. Witwer KW, et al. Defining mesenchymal stromal cell (MSC)-derived small extracellular vesicles for therapeutic applications. *Journal of Extracellular Vesicles*. 2019;8(1):1609206.
19. Chang HW, et al. Small extracellular vesicles from human adipose-derived stem cells attenuate cartilage degeneration. *Journal of Extracellular Vesicles*. 2020;9(1):1735249.
20. Minimal information for studies of extracellular vesicles 2018 (MISEV2018): a position statement of the International Society for Extracellular Vesicles and update of the MISEV2014 guidelines. *Journal of Extracellular Vesicles*. 2018;

21. Cheng L, et al. Focus on Mesenchymal Stem Cell-Derived Exosomes: Opportunities and Challenges in Cell-Free Therapy. *Stem Cells Int*. 2017;2017(6305295.
22. Yu B, Zhang XLi X. Exosomes derived from mesenchymal stem cells. *Int J Mol Sci*. 2014;15(3):4142-57.
23. Ferguson SW, et al. The microRNA regulatory landscape of MSC-derived exosomes: a systems view. *Sci Rep*. 2018;8(1):1419.
24. Harrell CR, et al. Mesenchymal Stem Cell-Derived Exosomes and Other Extracellular Vesicles as New Remedies in the Therapy of Inflammatory Diseases. *Cells*. 2019;8(12):
25. Heldring N, et al. Therapeutic Potential of Multipotent Mesenchymal Stromal Cells and Their Extracellular Vesicles. *Hum Gene Ther*. 2015;26(8):506-17.
26. Chen M, et al. Adoptive transfer of human gingiva-derived mesenchymal stem cells ameliorates collagen-induced arthritis via suppression of Th1 and Th17 cells and enhancement of regulatory T cell differentiation. *Arthritis Rheum*. 2013;65(5):1181-93.
27. Luo Y, et al. Human gingival tissue-derived MSC suppress osteoclastogenesis and bone erosion via CD39-adenosine signal pathway in autoimmune arthritis. *EBioMedicine*. 2019;43(620-631.
28. Wu W, et al. CD39 Produced from Human GMSCs Regulates the Balance of Osteoclasts and Osteoblasts through the Wnt/β-Catenin Pathway in Osteoporosis. *Mol Ther*. 2020;28(6):1518-1532.
29. Chen J, et al. TGF-β-induced CD4+ FoxP3+ regulatory T cell-derived extracellular vesicles modulate Notch1 signaling through miR-449a and prevent collagen-induced arthritis in a murine model. *Cell Mol Immunol*. 2021;18(11):2516-2529.
30. Théry C, et al. Isolation and characterization of exosomes from cell culture supernatants and biological fluids. *Curr Protoc Cell Biol*. 2006;Chapter 3(Unit 3.22.
31. Gardiner C, et al. Techniques used for the isolation and characterization of extracellular vesicles: results of a worldwide survey. *J Extracell Vesicles*. 2016;5(32945.
32. Li-Yan, et al. [Regulatory Effect of Exosomes Derived from Human Umbiilcal Cord Mesenchymal Stem Cells on Treg and TH17 Cells]. *Zhongguo Shi Yan Xue Ye Xue Za Zhi*. 2019;27(1):221-226.
33. Rani S, et al. Mesenchymal Stem Cell-derived Extracellular Vesicles: Toward Cell-free Therapeutic Applications. *Molecular Therapy the Journal of the American Society of Gene Therapy*. 2015;23(5):812.
34. Ji H, et al. Hepatitis-associated Aplastic Anemia Treated Successfully With Antithymocyte Globulin. *J Pediatr Hematol Oncol*. 2018;40(6):e355-e358.
35. Brand DD, Latham KARosloniec EF. Collagen-induced arthritis. *Nat Protoc*. 2007;2(5):1269-75.
36. Chen X, et al. Sodium butyrate regulates Th17/Treg cell balance to ameliorate uveitis via the Nrf2/HO-1 pathway. *Biochem Pharmacol*. 2017;142(111-119.
37. Chen W, et al. Apremilast Ameliorates Experimental Arthritis via Suppression of Th1 and Th17 Cells and Enhancement of CD4(+)Foxp3(+) Regulatory T Cells Differentiation. *Front Immunol*. 2018;9(1662.
38. Xiao ZX, Miller JSZheng SG. An updated advance of autoantibodies in autoimmune diseases. *Autoimmun Rev*. 2021;20(2):102743.
39. Valadi H, et al. Exosome-mediated transfer of mRNAs and microRNAs is a novel mechanism of genetic exchange between cells. *Nat Cell Biol*. 2007;9(6):654-9.
40. Lepeltier E, et al. Nanomedicine to target multidrug resistant tumors. *Drug resistance updates : reviews and commentaries in antimicrobial and anticancer chemotherapy*. 2020;52(100704.
41. Ludwig S, et al. mRNA and miRNA Profiles of Exosomes from Cultured Tumor Cells Reveal Biomarkers Specific for HPV16-Positive and HPV16-Negative Head and Neck Cancer. *International journal of molecular sciences*. 2020;21(22):
42. Staal FJT, Luis TCTiemessen MM. WNT signalling in the immune system: WNT is spreading its wings. *Nature Reviews Immunology*. 2008;8(8):581-593.
43. Li QVerma IM. NF-kappaB regulation in the immune system. *Nat Rev Immunol*. 2002;2(10):725-34.
44. Zhou Y, et al. Nuclear Factor κB (NF-κB)-Mediated Inflammation in Multiple Sclerosis. *Front Immunol*. 2020;11(391.
45. Calin GACroce CM. MicroRNA signatures in human cancers. *Nat Rev Cancer*. 2006;6(11):857-66.
46. Ferrara JL, et al. Graft-versus-host disease. *Lancet*. 2009;373(9674):1550-61.
47. Huang F, et al. Human Gingiva-Derived Mesenchymal Stem Cells Inhibit Xeno-Graft-versus-Host Disease via CD39-CD73-Adenosine and IDO Signals. *Front Immunol*. 2017;8(68.
48. Zhao J, et al. A preclinical study-systemic evaluation of safety on mesenchymal stem cells derived from human gingiva tissue. *Stem Cell Res Ther*. 2019;10(1):165.

49. Zhou Y, et al. Microstructure and mechanical behaviors of tibia for collagen-induced arthritic mice treated with gingiva-derived mesenchymal stem cells. *J Mech Behav Biomed Mater*. 2021;124(104719.
50. Wu W, et al. B7-H1 Promotes the Functional Effect of Human Gingiva-Derived Mesenchymal Stem Cells on Collagen-Induced Arthritis Murine Model. *Mol Ther*. 2020;28(11):2417-2429.
51. Dang J, et al. Human gingiva-derived mesenchymal stem cells are therapeutic in lupus nephritis through targeting of CD39(-)CD73 signaling pathway. *J Autoimmun*. 2020;113(102491.
52. Zhao J, et al. Human gingiva tissue-derived MSC ameliorates immune-mediated bone marrow failure of aplastic anemia via suppression of Th1 and Th17 cells and enhancement of CD4+Foxp3+ regulatory T cells differentiation. *Am J Transl Res*. 2019;11(12):7627-7643.
53. Zhang X, et al. Human Gingiva-Derived Mesenchymal Stem Cells Modulate Monocytes/Macrophages and Alleviate Atherosclerosis. *Front Immunol*. 2018;9(878.
54. Zhang W, et al. Human Gingiva-Derived Mesenchymal Stem Cells Ameliorate Streptozoticin-induced T1DM in mice via Suppression of T effector cells and Up-regulating Treg Subsets. *Sci Rep*. 2017;7(1):15249.
55. Yamaoka E, et al. Neoplastic transformation by TERT in FGF-2-expanded human mesenchymal stem cells. *Int J Oncol*. 2011;39(1):5-11.
56. Redaelli S, et al. From cytogenomic to epigenomic profiles: monitoring the biologic behavior of in vitro cultured human bone marrow mesenchymal stem cells. *Stem Cell Res Ther*. 2012;3(6):47.
57. Rosland GV, et al. Long-term cultures of bone marrow-derived human mesenchymal stem cells frequently undergo spontaneous malignant transformation. *Cancer Res*. 2009;69(13):5331-9.
58. Zhou J, et al. Mesenchymal Stem Cell Derived Exosomes in Cancer Progression, Metastasis and Drug Delivery: A Comprehensive Review. *J Cancer*. 2018;9(17):3129-3137.
59. Xu JF, et al. Altered microRNA expression profile in exosomes during osteogenic differentiation of human bone marrow-derived mesenchymal stem cells. *PLoS One*. 2014;9(12):e114627.
60. Cosenza S, et al. Mesenchymal stem cells-derived exosomes are more immunosuppressive than microparticles in inflammatory arthritis. *Theranostics*. 2018;8(5):1399-1410.
61. Chen Z, et al. Therapeutic Potential of Mesenchymal Cell-Derived miRNA-150-5p-Expressing Exosomes in Rheumatoid Arthritis Mediated by the Modulation of MMP14 and VEGF. *J Immunol*. 2018;201(8):2472-2482.
62. Bai L, et al. Effects of Mesenchymal Stem Cell-Derived Exosomes on Experimental Autoimmune Uveitis. *Sci Rep*. 2017;7(1):4323.
63. Wang W, et al. The Th17/Treg imbalance and cytokine environment in peripheral blood of patients with rheumatoid arthritis. *Rheumatol Int*. 2012;32(4):887-93.
64. Kosmaczewska A, et al. [The role of Th1, Th17, and Treg cells in the pathogenesis of rheumatoid arthritis including anti-inflammatory action of Th1 cytokines]. *Postepy Hig Med Dosw (Online)*. 2011;65(397-403.
65. Hueber AJ, et al. Mast cells express IL-17A in rheumatoid arthritis synovium. *J Immunol*. 2010;184(7):3336-40.
66. Hot AMiossec P. Effects of interleukin (IL)-17A and IL-17F in human rheumatoid arthritis synoviocytes. *Ann Rheum Dis*. 2011;70(5):727-32.
67. Peng Y, et al. Mesenchymal stromal cells infusions improve refractory chronic graft versus host disease through an increase of CD5+ regulatory B cells producing interleukin 10. *Leukemia*. 2015;29(3):636-46.
68. Kim YH, et al. Interleukin (IL)-10 induced by CD11b(+) cells and IL-10-activated regulatory T cells play a role in immune modulation of mesenchymal stem cells in rat islet allografts. *Mol Med*. 2011;17(7-8):697-708.
69. Huang JH, et al. Systemic Administration of Exosomes Released from Mesenchymal Stromal Cells Attenuates Apoptosis, Inflammation, and Promotes Angiogenesis after Spinal Cord Injury in Rats. *J Neurotrauma*. 2017;34(24):3388-3396.
70. Müller-Ladner U, et al. Synovial fibroblasts of patients with rheumatoid arthritis attach to and invade normal human cartilage when engrafted into SCID mice. *Am J Pathol*. 1996;149(5):1607-15.
71. Lefèvre S, et al. Synovial fibroblasts spread rheumatoid arthritis to unaffected joints. *Nat Med*. 2009;15(12):1414-20.
72. Zhu S, et al. Sonic hedgehog promotes synovial inflammation and articular damage through p38 mitogen-activated protein kinase signaling in experimental arthritis. *J Autoimmun*. 2022;132(102902.
73. Yang S, et al. Induced, but not natural, regulatory T cells retain phenotype and function following exposure to inflamed synovial fibroblasts. *Sci Adv*. 2020;6(44):

74. Schrepfer S, et al. Stem cell transplantation: the lung barrier. *Transplant Proc*. 2007;39(2):573-6.
75. Zangi L, et al. Direct imaging of immune rejection and memory induction by allogeneic mesenchymal stromal cells. *Stem Cells*. 2009;27(11):2865-74.
76. de Gassart A, et al. Lipid raft-associated protein sorting in exosomes. *Blood*. 2003;102(13):4336-44.
77. Wubbolts R, et al. Proteomic and biochemical analyses of human B cell-derived exosomes. Potential implications for their function and multivesicular body formation. *J Biol Chem*. 2003;278(13):10963-72.
78. Grange C, et al. Biodistribution of mesenchymal stem cell-derived extracellular vesicles in a model of acute kidney injury monitored by optical imaging. *Int J Mol Med*. 2014;33(5):1055-63.
79. Shen B, et al. CCR2 Positive Exosome Released by Mesenchymal Stem Cells Suppresses Macrophage Functions and Alleviates Ischemia/Reperfusion-Induced Renal Injury. *Stem Cells Int*. 2016;2016(1240301.
80. Chen J, et al. TGF-beta-induced CD4+ FoxP3+ regulatory T cell-derived extracellular vesicles modulate Notch1 signaling through miR-449a and prevent collagen-induced arthritis in a murine model. *Cell Mol Immunol*. 2021;18(11):2516-2529.
81. Chandra S, et al. Role of miRNAs in development and disease: Lessons learnt from small organisms. *Life Sci*. 2017;185(8-14.
82. Fang S-B, et al. Small extracellular vesicles derived from human mesenchymal stromal cells prevent group 2 innate lymphoid cell-dominant allergic airway inflammation through delivery of miR-146a-5p.
83. Mookherjee NEl-Gabalawy HS. High degree of correlation between whole blood and PBMC expression levels of miR-155 and miR-146a in healthy controls and rheumatoid arthritis patients. *J Immunol Methods*. 2013;400-401(106-10.
84. Y X, et al. Association of microRNAs genes polymorphisms with arthritis: a systematic review and meta-analysis. *Bioscience reports*. 2019;39(7):
85. GA C, et al. Human microRNA genes are frequently located at fragile sites and genomic regions involved in cancers. *Proceedings of the National Academy of Sciences of the United States of America*. 2004;101(9):2999-3004.
86. Chen G, et al. The NF-κB transcription factor c-Rel is required for Th17 effector cell development in experimental autoimmune encephalomyelitis. *Journal of Immunology*. 2011;187(9):4483.
87. Trentham DE, Townes ASKang AH. Autoimmunity to type II collagen an experimental model of arthritis. *J Exp Med*. 1977;146(3):857-68.
88. Kong N, et al. Induced T regulatory cells suppress osteoclastogenesis and bone erosion in collagen-induced arthritis better than natural T regulatory cells. *Ann Rheum Dis*. 2012;71(9):1567-1572.
89. Kong N, et al. Antigen-specific transforming growth factor beta-induced Treg cells, but not natural Treg cells, ameliorate autoimmune arthritis in mice by shifting the Th17/Treg cell balance from Th17 predominance to Treg cell predominance. *Arthritis Rheum*. 2012;64(8):2548-58.
90. Joosten LA, et al. Anticytokine treatment of established type II collagen-induced arthritis in DBA/1 mice: a comparative study using anti-TNFalpha, anti-IL-1alpha/beta and IL-1Ra. *Arthritis Rheum*. 2008;58(2 Suppl):S110-22.
91. Sutton EJ, et al. An optical imaging method to monitor stem cell migration in a model of immune-mediated arthritis. *Opt Express*. 2009;17(26):24403-13.
92. Lu L, et al. Critical role of all-trans retinoic acid in stabilizing human natural regulatory T cells under inflammatory conditions. *Proc Natl Acad Sci U S A*. 2014;111(33):E3432-40.
93. Lefèvre S, et al. Synovial fibroblasts spread rheumatoid arthritis to unaffected joints. *Nature Medicine*. 2009;15(12):1414.

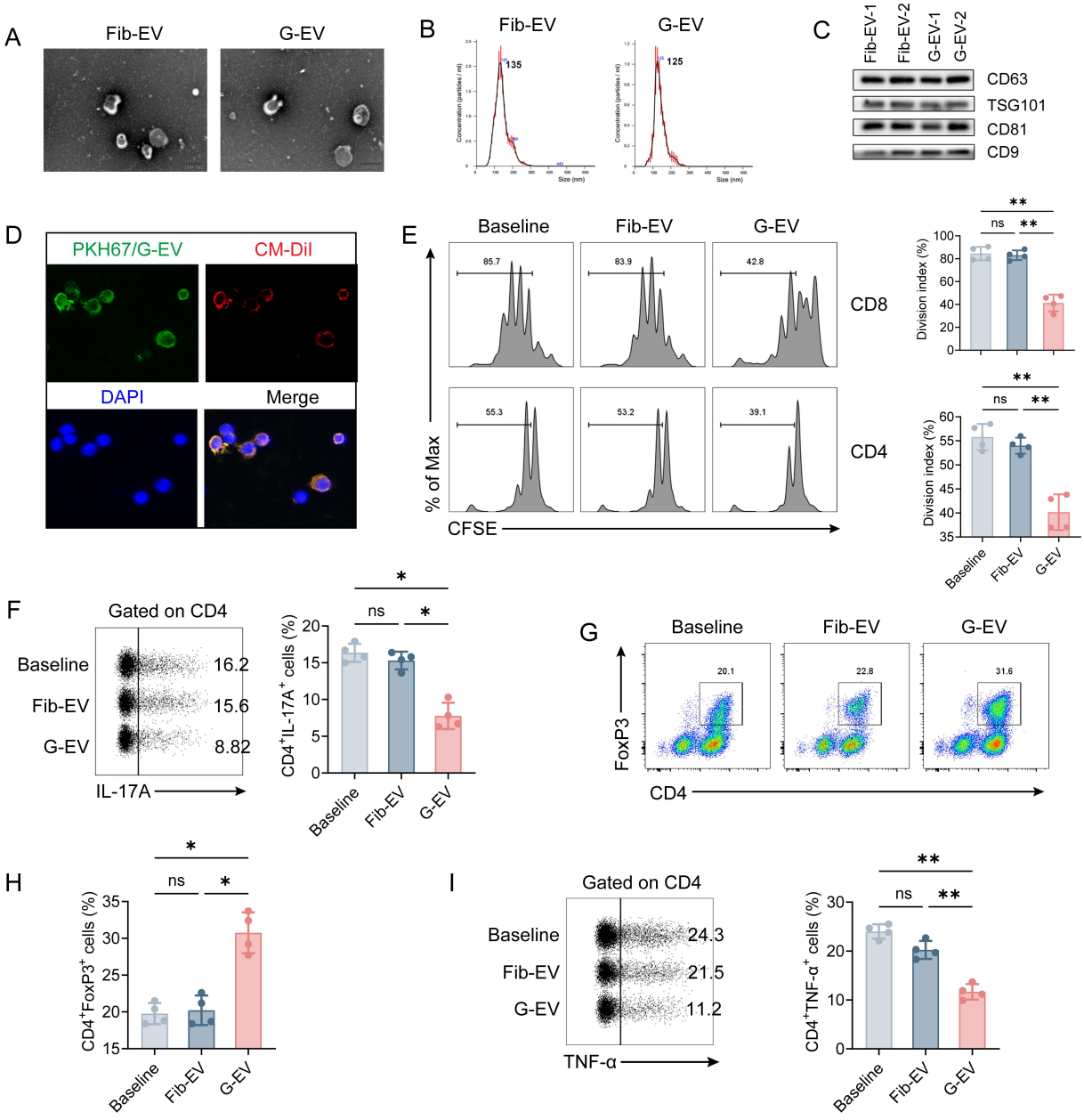

Figure 1. Human GMSC-derived EVs inhibit T-cell responses *in vitro*. **(A)** Electron micrograph analysis of the morphology of EVs. Scale bar, 200 nm. **(B)** Nanoparticle trafficking analyzed the diameters and concentration of EVs. **(C)** The EVs' protein markers were detected by Western blot. **(D)** PKH67-labelled (green) GMSC-EVs were co-cultured with CD3+ T cells under stimulation of soluble anti-CD3 and soluble anti-CD28 Abs after 1 days, cells were harvested and stained with CM-DiI (Red) and DAPI (Blue), then images were acquired by fluorescence confocal. **(E)** *In vitro* suppressive assay of T cell proliferation. **(F)** Th17-polarizing analysis. **(G, H)** Treg-polarizing analysis. **(I)** *In vitro* suppressive assay of cytokine production. Statistical significance was assessed ANOVA with Dunnett multiple comparison test in E-I. Data are shown as the means ± SD from one of three independent experiments. *, $p < 0.05$; **, $p < 0.01$.

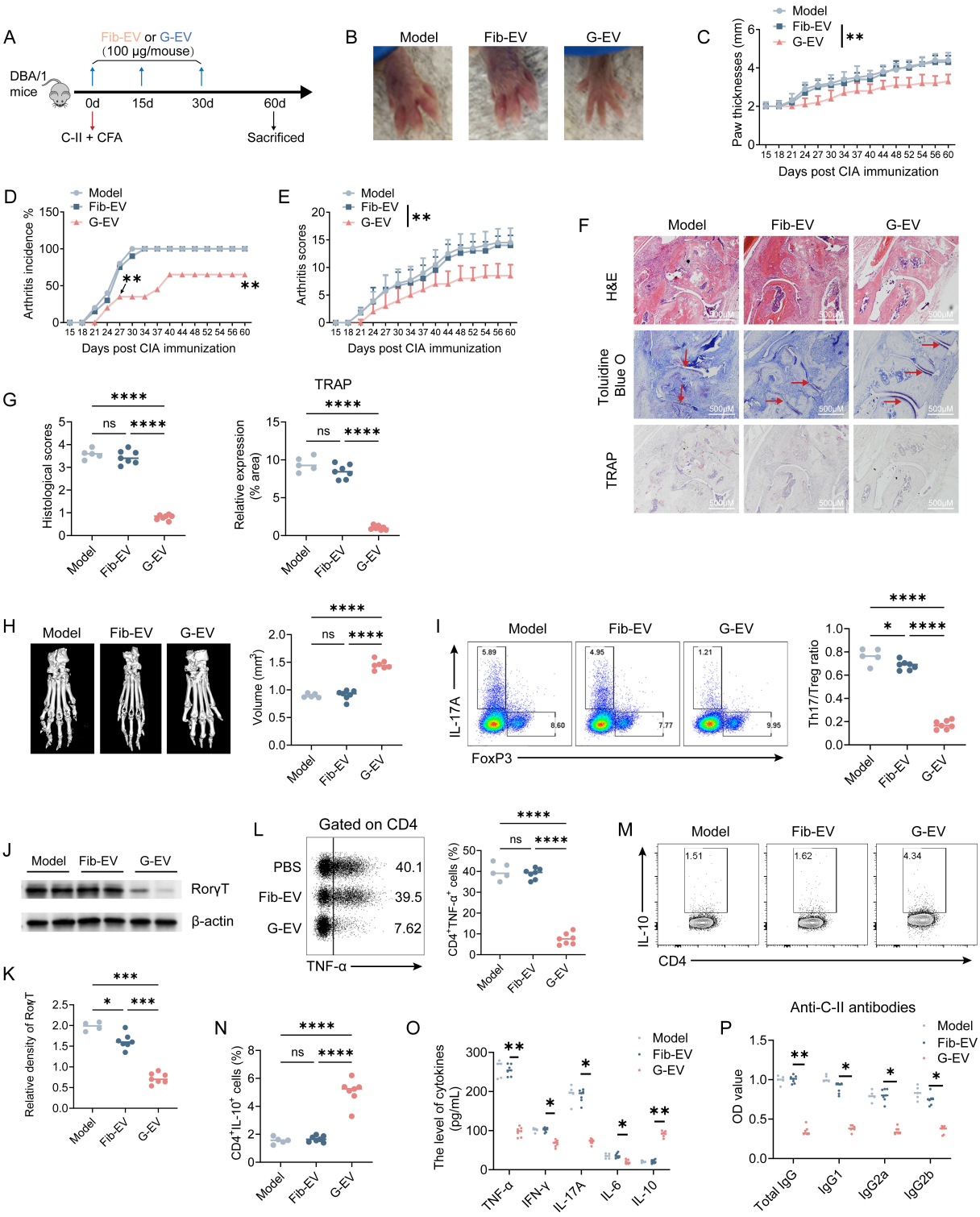

Figure 2. Human GMSC-derived EVs protect against collagen-induced arthritis (CIA) model. (A) Schematic diagram summarized the CIA modeling and G-EVs administration. **(B)** The representative images of gross appearance of swollen hind paws at the endpoint of the experiment. The paw thickness **(C)**, incidence of arthritis **(D)** and arthritis severity scores **(E)** of CIA mice were monitored from day 15 to day 60 post immunization. **(F, G)** Ankle joint

sections isolated from CIA mice at day 60 post immunization were stained with hematoxylin and eosin (H&E) and toluidine blue staining. Histopathologic scores were evaluated for features of synovitis, pannus, erosion and cartilage matrix. The red arrows indicated the cartilage destruction of joints. Osteoclast distribution was quantified by tartrate acid resistant phosphatase (TRAP) staining. **(H)** Toe joint sections isolated from CIA mice at day 60 post immunization were imaged with micro-CT and the structural damage were evaluated as bone volumes of the metatarsophalangeal joint indicated. **(I)** dLNs cells isolated from CIA mice at day 60 post immunization for intracellular staining of IL-17A and Foxp3 by flow cytometry analysis. **(J, K)** Splenic cells isolated from CIA mice at day 60 post immunization were collected for the detection of the protein level of RorγT by Western blot analysis. **(L-N)** dLNs isolated from CIA mice at day 60 post immunization for intracellular staining of TNF-α and IL-10 in CD4+ cells by flow cytometry analysis. Serum samples obtained from blood of CIA mice at day 60 post immunization were used for the detection of cytokines **(O)** and autoantibodies **(P)** by ELISA assays. Statistical significance was assessed ANOVA with Dunnett multiple comparison test in C-P. Data are mean ± SD, n = 5-8 mice. *, $p < 0.05$; **, $p < 0.01$; ***, $p < 0.001$; ****, $p < 0.0001$.

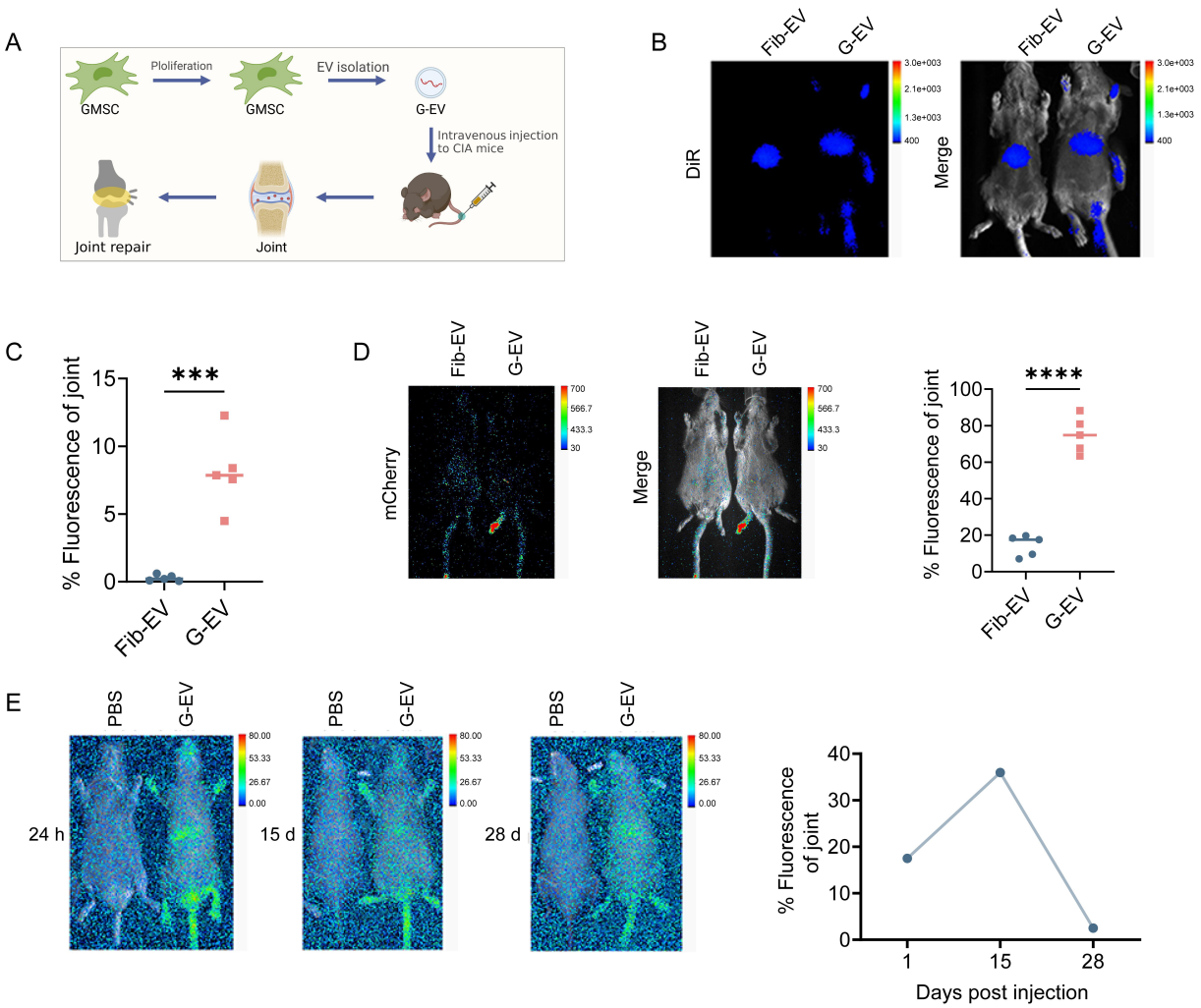

Figure 3. *In vivo* tracking of human GMSC-derived EVs in CIA mice. **(A)** Schematic illustration depicting the delivery of EVs to the joint *via* the tail vein for the treatment of CIA. **(B)** 24 h following the administration of DiR-labelled (Red) EVs in CIA mice 2, digital photo and IVIS images were used to present the fluorescence signal. **(C)** Quantification of fluorescence percentage of joint in total for (B). **(D)** *In vivo* imaging of mCherry-carried (Red) EVs in CIA mice 24 h post injection, and quantification of fluorescence percentage of joint in total. **(E)** *In vivo* imaging of DiR-labelled GMSC-EVs in CIA mice at 24 h, 14 days and 28 days post injection, and quantification of fluorescence percentage of joint in total. Left mouse received PBS as the control. Statistical significance was assessed with two-tailed Student t test in C and D. Representative images from three separate experiments. ***, $p < 0.001$; ****, $p < 0.0001$.

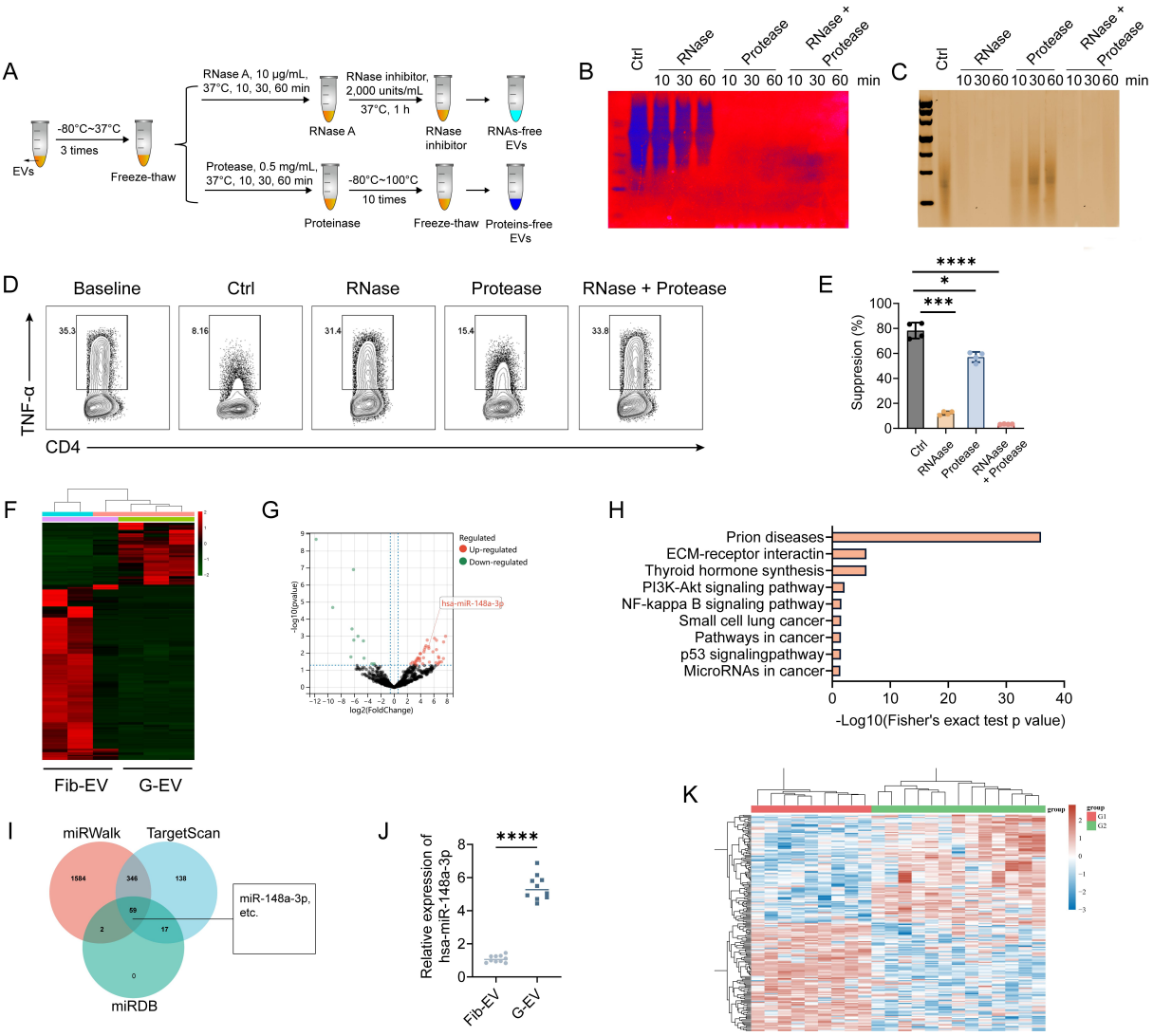

Figure 4. Bioinformatics analysis of the miRNA expression profile of human GMSC-derived EVs. **(A)** Flowchart illustrates the experimental procedures for removal of proteins or RNAs in GMSC-EVs. **(B)** Silver staining of polyacrylamide gel showed the protein profile GMSC-EVs upon different treatment procedures described in Methods. **(C)** The image of agarose gel showed the RNA profile GMSC-EVs upon different treatment procedures described in Methods. **(D, E)** *In vitro* suppressive assay of cytokine production. **(F)** The heatmap shows the miRNA expression profile of GMSC-EVs. **(G)** Volcano plot shows differentially expressed miRNAs. $p < 0.05$ and fold change ≥ 2 was considered statistically significant. **(H)** The pathway enrichment of the differentially expressed miRNAs was performed in online database DIANA-MirPath v.3. The x-axis represents -log10(p-value), the y-axis represents KEGG term; $p < 0.05$ was considered statistically significant. **(I)** The predicted miRNAs to regulate IKKB from different database TargetScan, miRWalk and miRDB. **(J)** The miR-148a-3p level in GMSC-EVs were measured by qPCR. **(K)** Heatmap of the differentially expressed genes in RA-related publicly available dataset GSE56649 (13

cases of RA and 9 healthy controls). Statistical significance was assessed ANOVA with Dunnett multiple comparison test in E and by two-tailed Student t test in J. Data are shown as the means ± SD from one of three independent experiments. *, $p < 0.05$; **, $p < 0.01$; ***, $p < 0.001$; ****, $p < 0.0001$.

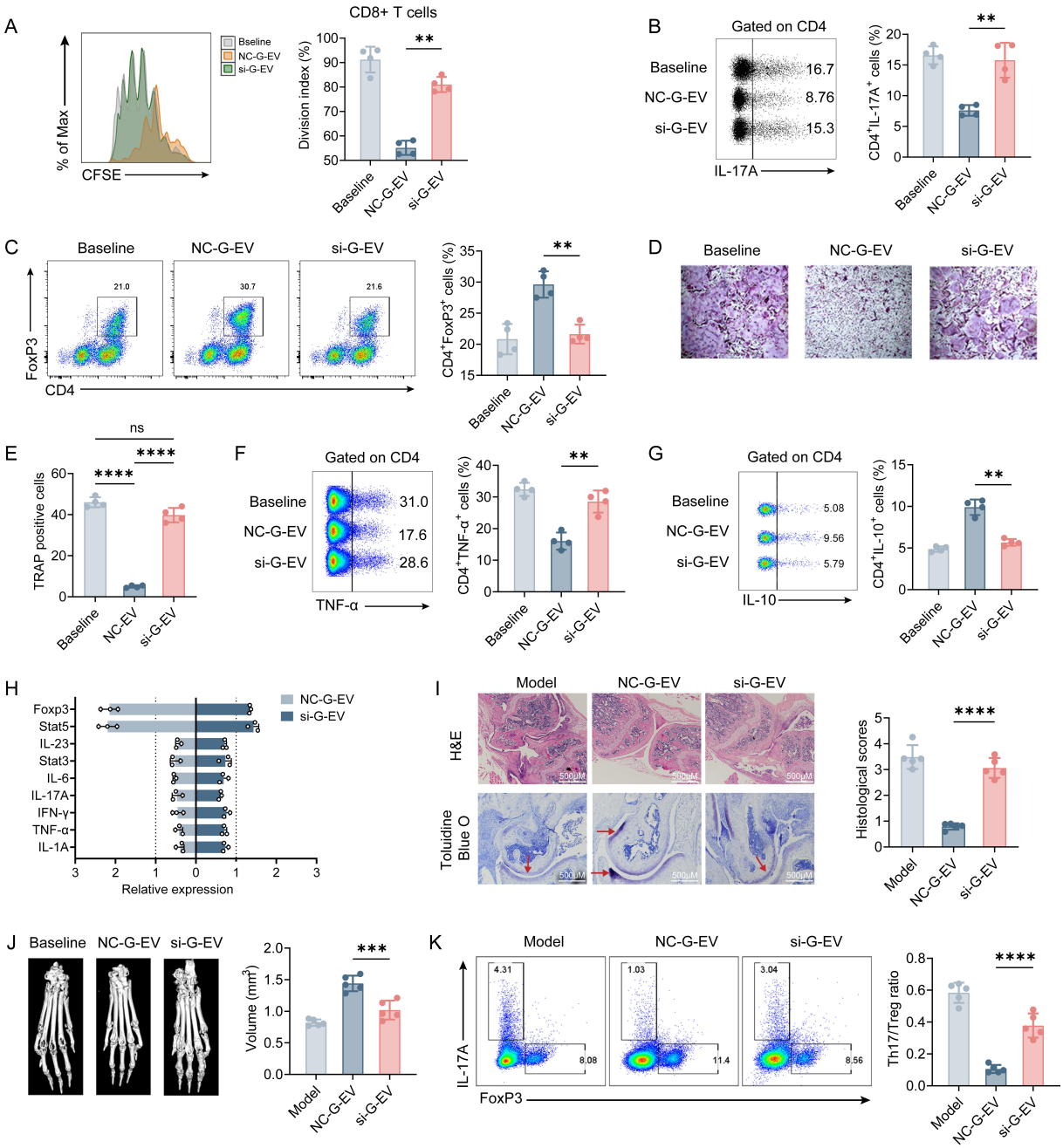

Figure 5. Blockage of miR-148a-3p in human GMSC-derived EVs disturbs the immunoregulatory properties. **(A)** *In vitro* suppressive assay of T cell proliferation. **(B, C)** *In vitro* Th17-polarizing and Treg-polarizing assays. **(D, E)** Representative images of osteoclast generation under different conditions. TRAP-positive osteoclast numbers of per area under different conditions were quantified. **(F, G)** *In vitro* suppressive assay of cytokine production. **(H)** qPCR for inflammation or tolerance phenotype of CD3+ T cells. **(I-K)** CIA mice received a single type of NC-GMSC-EVs or si-GMSC-EVs at day 0, 15 and 30 post immunization, and individual analysis was acquired at the endpoint of the experiment (Day 60 post immunization). **(I)** Knee joint sections were stained with H&E and toluidine blue

staining, and histopathologic scores were evaluated for features of synovitis, pannus, erosion and cartilage matrix. **(J)** Toe joint sections were imaged with micro-CT and bone volumes of the metatarsophalangeal joints were calculated. **(K)** Intracellular staining of IL-17A, and Foxp3 in dLNs were detected by flow cytometry analysis. Statistical significance was assessed ANOVA with Dunnett multiple comparison test in A-G, I-K and by two-tailed Student t test in H. A-H Data are shown as the means ± SD from one of three independent experiments. *, $p < 0.05$; **, $p < 0.01$; ***, $p < 0.001$; ****, $p < 0.0001$. I-K Data are mean ± SD, n = 5-8 mice. *, $p < 0.05$; **, $p < 0.01$; ***, $p < 0.001$; ****, $p < 0.0001$.

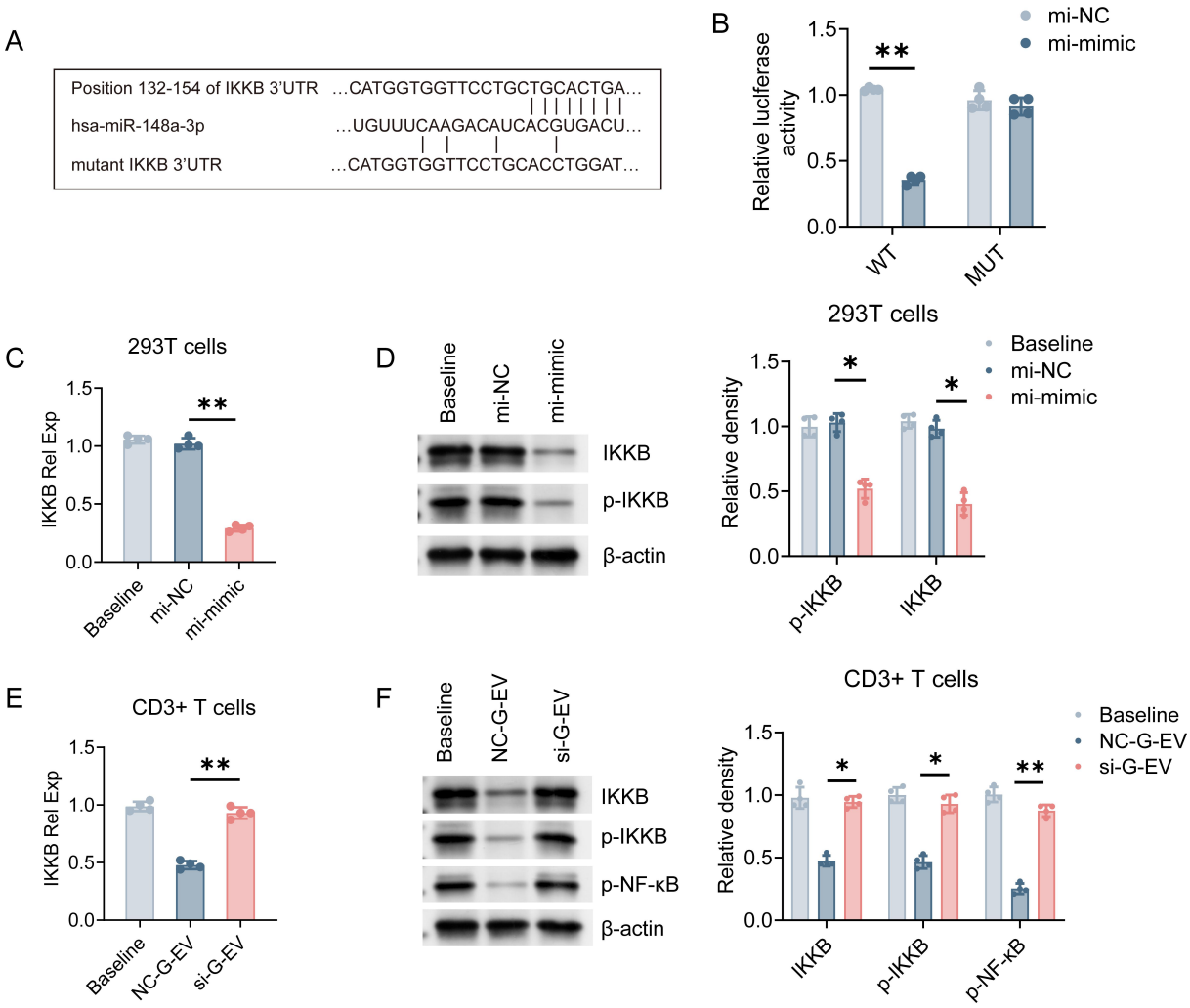

Figure 6. MiR-148a-3p-containing human GMSC-derived EVs modulate IKKB-NF-κB signaling pathway. (A) Sequence alignment of miR-148a-3p and its putative target sites in the 3'-UTR of IKKB mRNA. Mutation was generated in the complementary sites for the seed region of miR-148a-3p, as indicated. **(B)** HEK-293T cells were transiently co-transfected with IKKB WT or mutant 3' UTR luciferase reporter plasmid and miR-148a-3p mimic for 48 h, and luciferase activity was analyzed. **(C, D)** HEK-293T cells were transiently transfected with negative control or miR-148a-3p mimic. Cells were collected at 48 h and the expression of IKKB or p-IKKB were detected by qPCR or Western blot respectively. **(E, F)** CD3+ T cells isolated from C57BL/6 mice were co-cultured with NC-GMSC-EVs or si-GMSC-EVs under the activated condition. Cells were collected at 72 h and the expression of IKKB, p-IKKB and p-NF-κB were detected by qPCR or Western blot respectively. Statistical significance was assessed ANOVA with Dunnett multiple comparison test in C-F and by two-tailed Student t test in B. Data are shown as the means ± SD from one of three independent experiments. *, $p < 0.05$; **, $p < 0.01$.

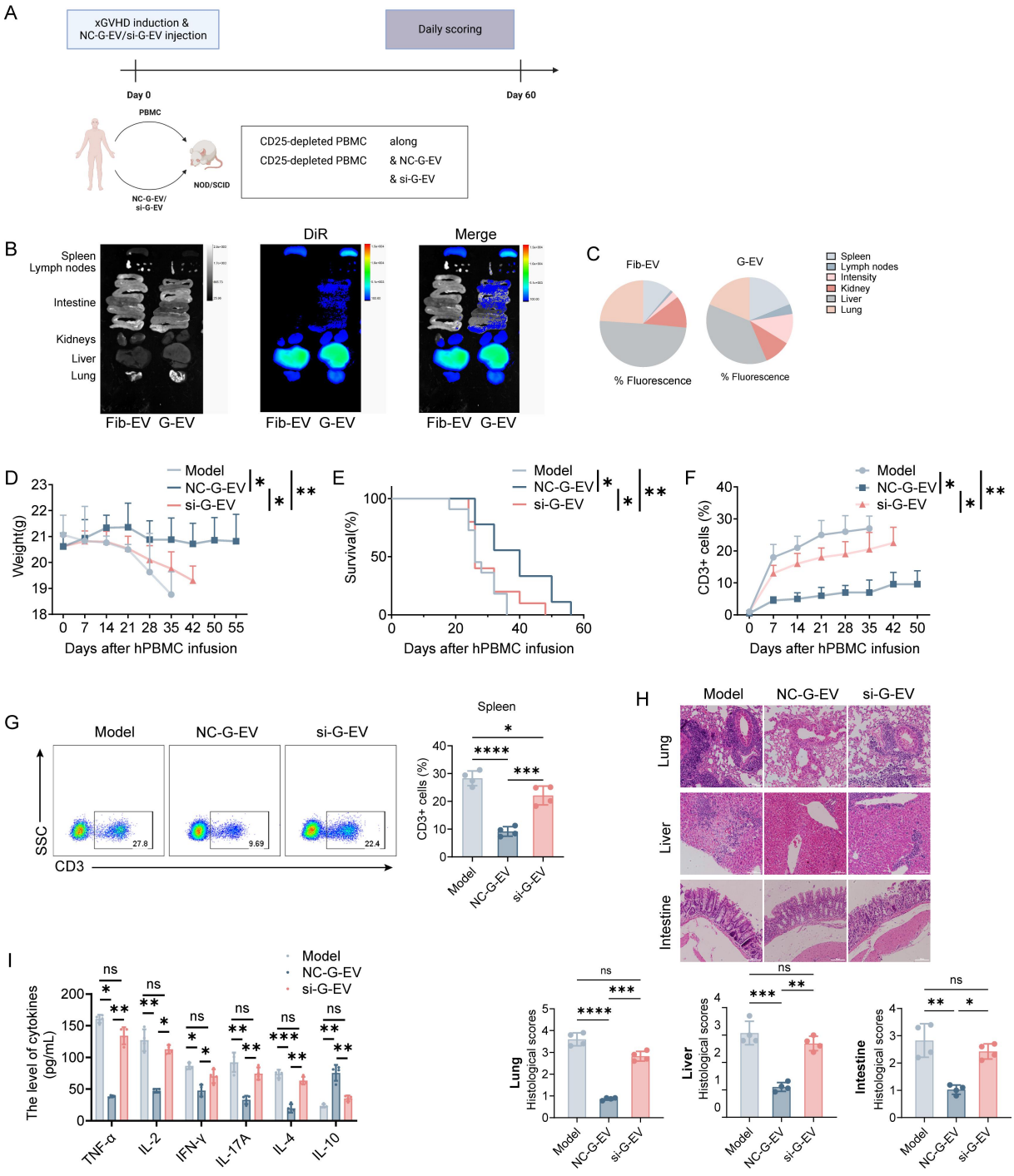

Figure 7. Impact of GMSC-derived EVs on xGvHD model *in vivo*. (A) Schematic experimental set-up for xGvHD**. (B)** Following the administration of DiR-labelled (Red) EVs injections to the xGvHD mice, digital photographs and IVIS images were used to present the major organs. **(C)** Quantification of fluorescence percentage of organs for (B). **(D-I)** xGvHD mice were received with NC-GMSC-EVs or si-GMSC-EVs at day 0, 15 and 30. The survival **(D)**, weight **(E)** and human CD3+ T cells in peripheral blood **(F)** of xGvHD mice were monitored from day 15 to day 60. **(G)** dLNs isolated from xGvHD mice at the 50th days was used to determine the human CD3+ percentage by flow cytometry analysis. **(H)** Liver, lung,

intestine of NOD/SCID mice collected at the 50th days were stained with H&E and histopathologic severity scores were determined by lymphocyte invasion. **(I)** Sera were collected from blood of NOD/SCID mice at the 50th day, and the levels of TNF-α, IL-2, IFN-γ, IL-17A, IL-4, and IL-10 were detected by ELISA assays. B, C Representative *in vivo* tracking images from three separated experiments. Statistical significance was assessed ANOVA with Dunnett multiple comparison test in D, F-I and by log-rank test in E. D-I Data are mean ± SD, n = 10 mice. *, $p < 0.05$; **, $p < 0.01$; ***, $p < 0.001$; ****, $p < 0.0001$.

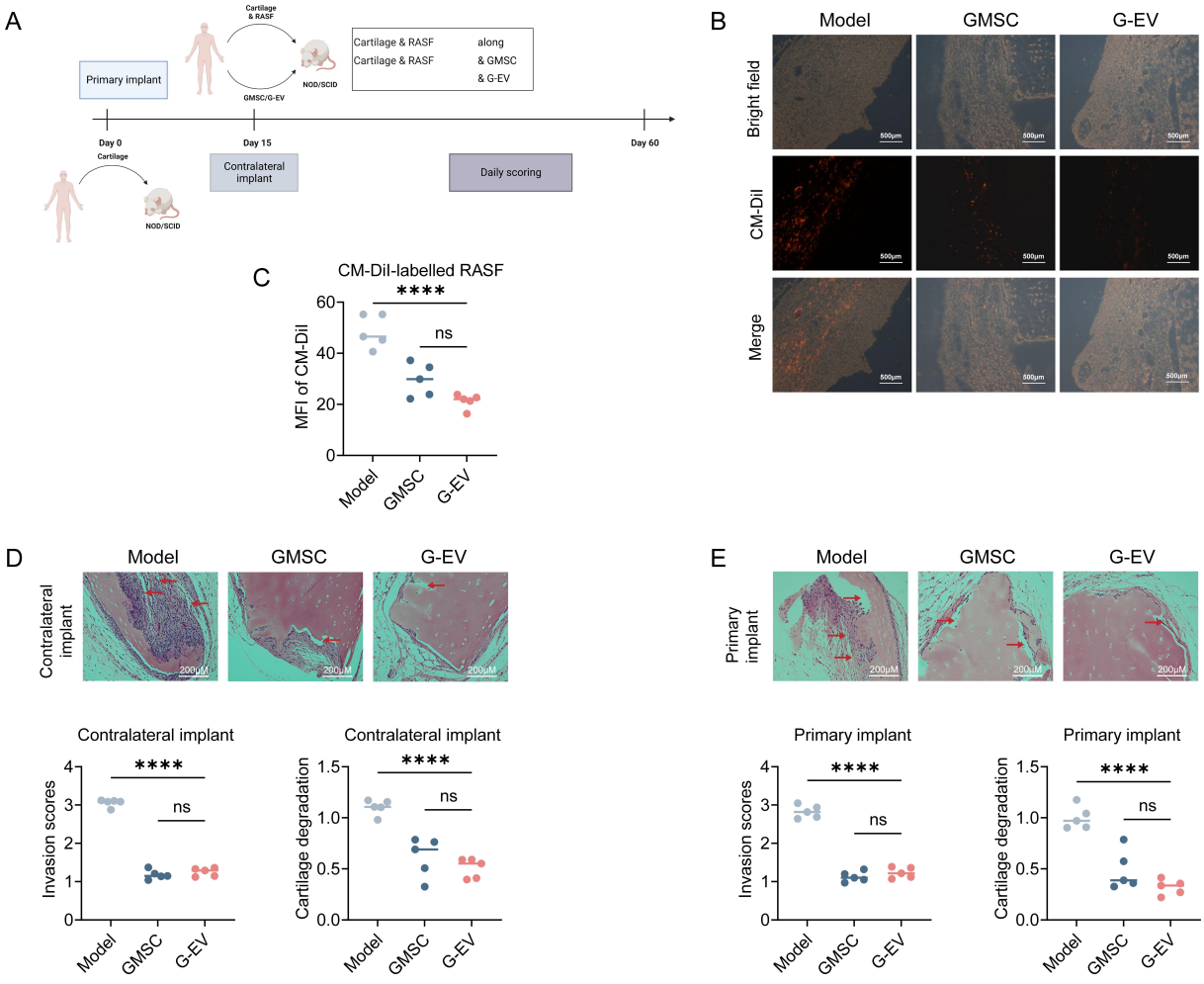

Figure 8. GMSC-derived EVs protect against inflamed synovial fibroblast-mediated humanized animal model. **(A)** Schematic experimental set-up for RASFs-mediated humanized animal model. In the first operation, SCID mice were implanted with a cartilage-sponge complex under the left flank skin (primary implant). After two weeks, individual 5×10^5 CM-DiI-labeled RASFs, 2×10^6 GMSCs and/or 100 μg GMSC-EVs were injected into the cartilage-sponge complex, and the implant was inserted into a subcutaneous space in the right flank skin (contralateral implant). At day 60, the primarily and contralateral cartilages were collected, and the mean fluorescence intensity (MFI) of CM-DiI-labelled RASFs in primarily cartilages were quantified using Image J software to evaluate the invasiveness of contralateral RASFs after treatment with GMSCs or GMSC-EVs **(B, C)**. The contralateral and primary cartilages were collected and subjected to H&E staining to assess the invasiveness scores of inflammatory cells and the destruction of cartilages **(D, E)**. The red arrows indicated the lesions of cartilage destruction caused by RASFs. Statistical significance was assessed ANOVA with Dunnett multiple comparison test in B-E. Data are mean ± SD, n = 5-6 mice. ****, $p < 0.0001$.